

CHAPTER III

RESULTS AND DISCUSSION


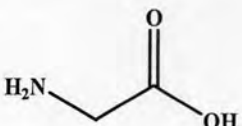
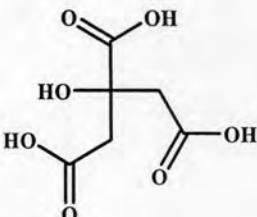
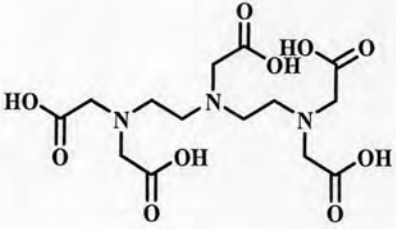
In this research, perovskite compounds $\text{Ba}_{0.5}\text{Sr}_{0.5}\text{Co}_{0.8}\text{Fe}_{0.2}\text{O}_{3-\delta}$, $\text{La}_{0.7}\text{Sr}_{0.3}\text{Ga}_{0.7}\text{Fe}_{0.2}\text{Mg}_{0.1}\text{O}_{3-\delta}$, $\text{La}_{0.8}\text{Sr}_{0.2}\text{Ga}_{0.8}\text{Mg}_{0.15}\text{Co}_{0.05}\text{O}_{3-\delta}$, PrSrCoO_4 , PrSrNiO_4 were synthesized by sol gel and hydrothermal method using various chelating agents such as citric acid, glycine, diethylenetriaminepentaacetic acid, citric acid-glycine and ethylene glycol-citric acid.

3.1 Synthesis of perovskite oxides

3.1.1 Sol gel method

Perovskite oxides powders were synthesized by sol gel method with various chelating agents (Table 2.3) and their structures are shown in Table 3.1. Sol-gel process involves producing precursor from chelating agents and metal nitrate/acetates before thermal decomposition. The process consists of three major steps (1) the metal cations react with ligands to form metal-chelate complexes at room temperature; (2) when $\text{NH}_3\cdot\text{H}_2\text{O}$ was added ($\text{pH} \approx 9$), the metal chelate complex undergoes crosslinking and turned into a polymer chain structure [27]. Meanwhile $\text{NH}_3\cdot\text{H}_2\text{O}$ was added, the white fume of NH_4NO_3 was suddenly observed, which came from the free NO_3^- reacting with $\text{NH}_3\cdot\text{H}_2\text{O}$. (3) after heating up at $\sim 100^\circ\text{C}$, thus solution turned into gel.

Table 3.1 Chelating agent structure

Chelating agents	Structure
Ethylene glycol	
Glycine	
Citric acid	
Diethylenetriaminepenta acetic acid (H ₅ DTPA)	

3.1.2 Hydrothermal method

The metal-chelated complex solution was prepared from the reaction of metal nitrates/acetates with chelating agents. After amount liquid ammonia was added dropwise to the aboved mixed solution. Then this solution was transferred to the autoclave and it was placed into an oven at 150°C. Then, it was aged for 20 hours. During the aging period, above reaction takes place to produce monomers, followed by nucleation and crystal growth [28]. Under ambient condition, syntheses are usually conducted at autogeneous pressure, which corresponds to the saturated vapor pressure of the solution at the specified temperature and composition of the hydrothermal solution. Thus, the polymerization reaction was enhanced. Moreover, the elimination/reduction of aggregates combined with narrow particle size distributions in the starting powders leads

to optimized and reproducible properties of ceramics because of better microstructure control [29].

Finally, the aqueous solution from both of sol gel and hydrothermal methods were heated up for combustion process. The combustion of metal citrate-nitrate gel solution was composed of three steps, evaporation, decomposition, and spontaneous combustion. The excess solvent was firstly evaporated until a sticky gel was obtained. Finally, around 200°C the spontaneous combustion occurred and the mixture was converted into the powder. The powder was heated up to 400°C for 2 hours to complete metal oxides formation. The synthesized perovskite oxides were grounded and sieved through 200 mesh (75 micron) for the high homogeneity of particles size. The uniform particles had effected to reducing of calcination temperatured to 900°C and sintered at 1100-1450°C.

3.2 Characterization of the perovskite compounds

As-synthesized powder was calcined to remove residual water and other impurities. In case of sintering process, the effect of heat treatment is related to improve crystallized structure and the fusing of particles to increase the density of the perovskite disc and eliminate the pores.

The structures of synthesized perovskite compounds were characterized by XRD and the surface morphology by SEM.

3.2.1 X-ray diffraction (XRD)

The phase formations of perovskites were characterized after calcinations. The diffraction peaks of perovskites were observed within 2θ in the range of 20 to 70°.

3.2.1.1 Phase formation of BSCF (synthesized by sol gel method)

The XRD pattern of BSCF using various chelating agents showed single phase of perovskite oxides with cubic structure.

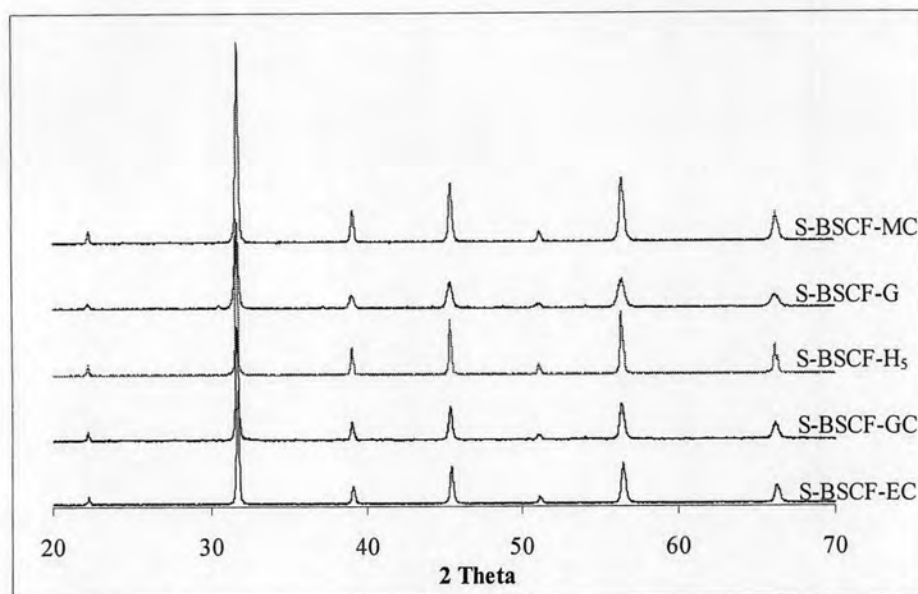


Figure 3.1 The XRD patterns of Ba_{0.5}Sr_{0.5}Co_{0.8}Fe_{0.2}O_{3-δ} powders synthesized by sol gel method using various chelating agents.

There is no significant shift of XRD peaks of BSCF powders synthesized by sol gel method using various chelating agents. In addition, the crystallite size calculated by using Scherrer formula was shown in Table 3.2. It was found that BSCF powders synthesized with H₅DTPA (S-BSCF-H₅) had the largest crystallite size.

Table 3.2 Crystallite sizes of synthesized BSCF powders by sol gel method with using different chelating agents

Perovskites	Crytrallite size (nm)
S-BSCF-MC	49
S-BSCF-G	56
S-BSCF-H ₅	76
S-BSCF-GC	49
S-BSCF-EC	53

3.2.1.2 Phase formation of $Ba_{0.5}Sr_{0.5}Co_{0.8}Fe_{0.2}O_{3-\delta}$ (synthesized by hydrothermal method)

The XRD pattern indicated that all the prepared BSCF samples had a single cubic perovskites phase [44].

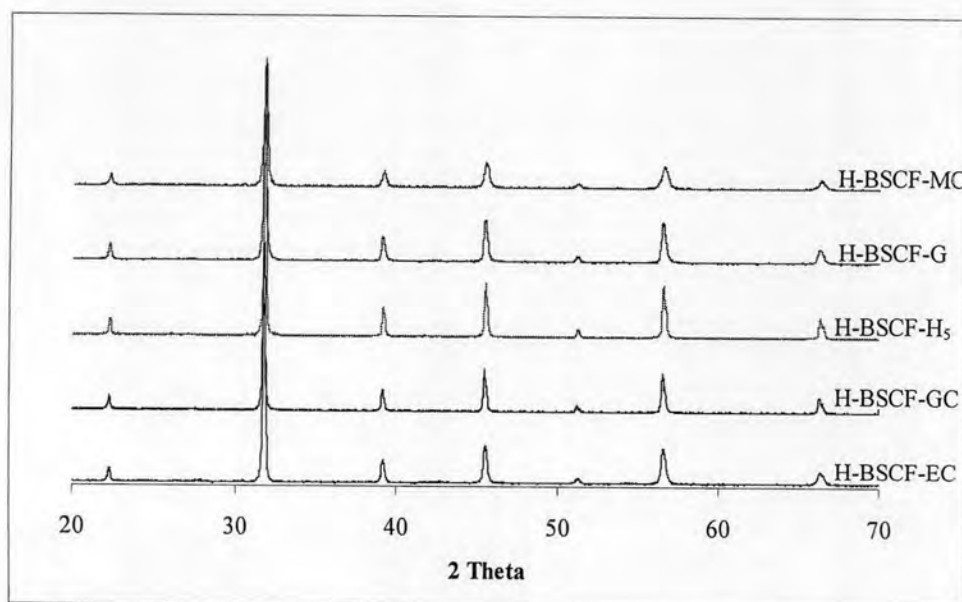


Figure 3.2 The XRD patterns of $Ba_{0.5}Sr_{0.5}Co_{0.8}Fe_{0.2}O_{3-\delta}$ powders synthesized by hydrothermal method using various chelating agents.

Table 3.3 showed that the crystallite size of the BSCF powders synthesized by hydrothermal method was smaller than that obtained from sol gel method. It is explained that hydrothermal method can control the rate and uniformity of nucleation, growth, aging and significantly reduced aggregation levels, that is not

possible with many other synthesis processes [29]. H-BSCF-MC has the smallest size of 31 nm. The result indicated that reaction under constant temperature (150°C) in autoclave provide good homogeneous mixing of metal cations with the chelating ligands with no aggregation during calcinations.

Table 3.3 Crystallite sizes of synthesized BSCF powders by hydrothermal method

	Perovskites	Crytrallite size (nm)	
using	H-BSCF-MC	31	different agents
chelating	H-BSCF-G	43	
	H-BSCF-H ₅	42	
	H-BSCF-GC	38	
	H-BSCF-EC	45	

It is noted that the crystallite size of H-BSCF-H₅ perovskite obtained is greatly reduced. Therefore, under ambient condition of hydrothermal method amorphous perovskite precursors were formed. The obtained precursors were easily to combustion. Thus, temperature and time of auto combustion was small which also reduced the particles agglomeration.

3.2.1.3 Phase formation of PrSrCoO₄ (synthesized by sol gel method)

XRD patterns of all samples of PrSrCoO₄ exhibited the single phase with tetragonal K₂NiF₄-type structure [45].

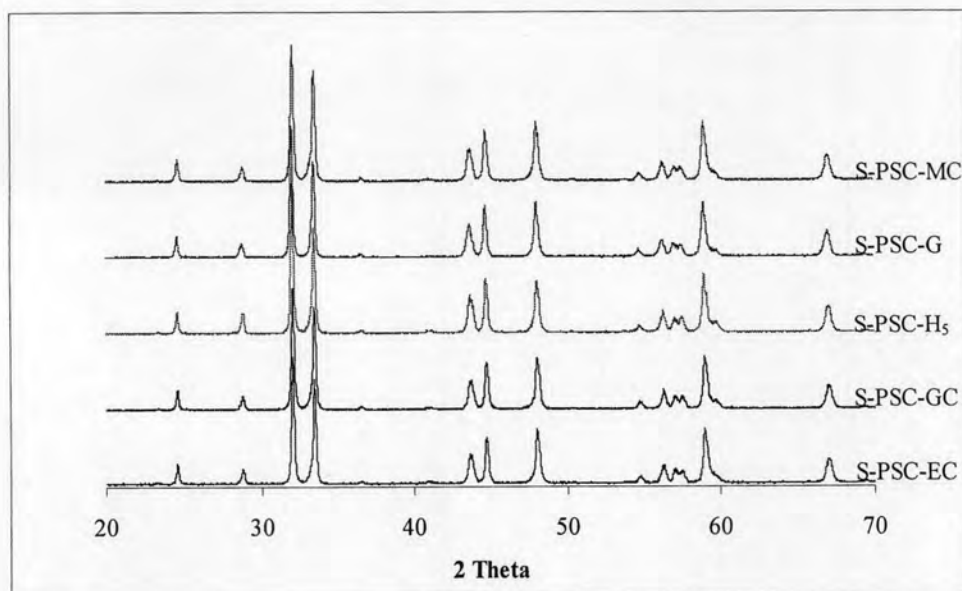


Figure 3.3 The XRD patterns of PrSrCoO₄ powders synthesized by sol gel method using various chelating.

It is seen in Table 3.4 that PSC powders had the slightly change in crystallite size.

Table 3.4 Crystallite sizes of synthesized PSC powders by sol gel method using different chelating agents

Perovskites	Crytrallite size (nm)
S-PSC-MC	42
S-PSC-G	49
S-PSC-H ₅	44
S-PSC-GC	40
S-PSC-EC	41

3.2.1.4 Phase formation of PrSrCoO₄ (synthesized by hydrothermal method)

The XRD patterns of PrSrCoO₄ in Figure 3.4 show the same result as Figure 3.3. PrSrCoO₄ has single phase with tetragonal K₂NiF₄-type structure.

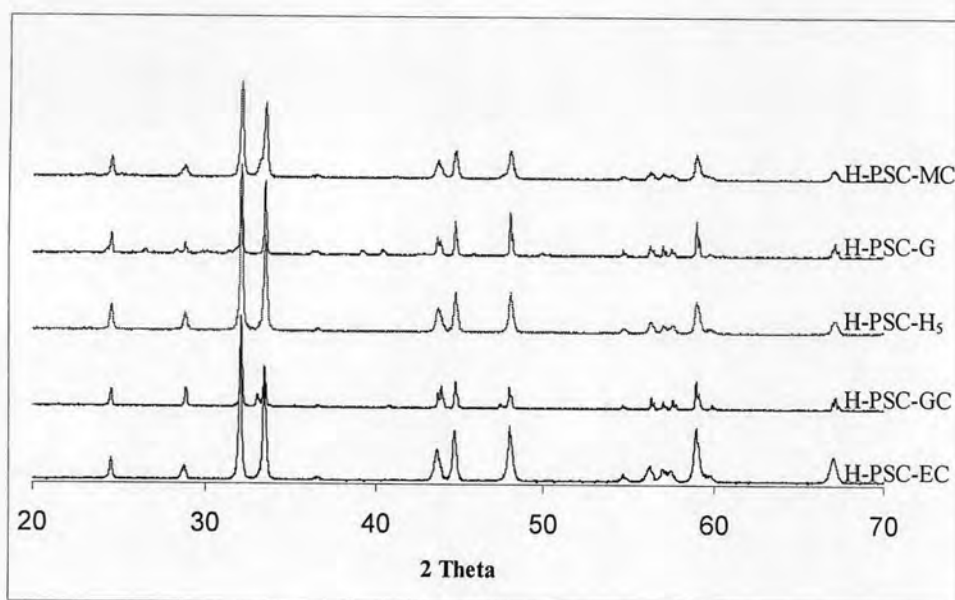


Figure 3.4 The XRD patterns of PrSrCoO₄ powders synthesized by hydrothermal method using various chelating agents.

Table 3.5 showed that the crystallite sizes of the oxides prepared by hydrothermal method decrease slightly as compared to those acquired by the sol gel method. It is suggested the synthesis method has no effect on the crystallite size. PSC synthesized by citric acid and ethylene glycol-citric acid as chelating agents have the smallest crystallite size of 39 nm.

Table 3.5 Crystallite sizes of synthesized PSC powders by hydrothermal method different chelating agents

Perovskites	Crytrallite size (nm)
H-PSC-MC	39
H-PSC-G	47
H-PSC-H ₅	41
H-PSC-GC	37
H-PSC-EC	39

3.2.1.5 Phase formation of PrSrNiO₄ (synthesized by sol gel method)

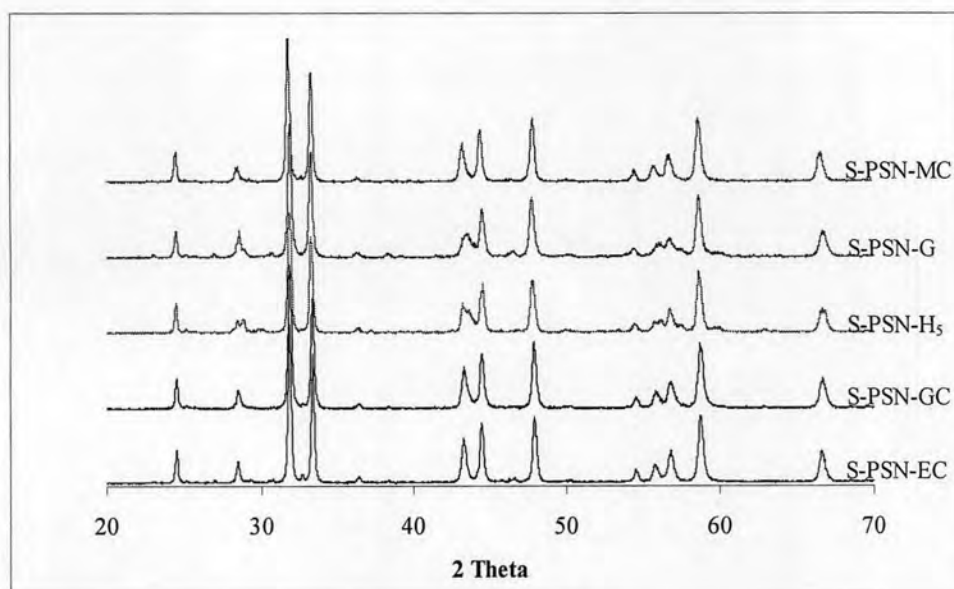


Figure 3.5 The XRD patterns of PrSrNiO₄ powders synthesized by sol gel method using various chelating agents.

The XRD patterns of the synthesized PrSrNiO₄ (Figure 3.5) showed that all the diffraction peaks belong to single phase with tetragonal K₂NiF₄-type structure. It was found that PSN powders synthesized using glycine as chelate had crystallite size of 32 nm (Table 3.6).

Table 3.6 Crystallite sizes of synthesized PSN powders by sol gel method using different chelating agents

Perovskites	Crytrallite size (nm)
S-PSN-MC	33
S-PSN-G	32
S-PSN-H ₅	39
S-PSN-GC	35
S-PSN-EC	34

3.2.1.6 Phase formation of PrSrNiO₄ (synthesized by hydrothermal method)

The XRD patterns of all PrSrNiO₄ (Figure 3.6) synthesized by hydrothermal method also showed single phase with tetragonal K₂NiF₄-type structure.

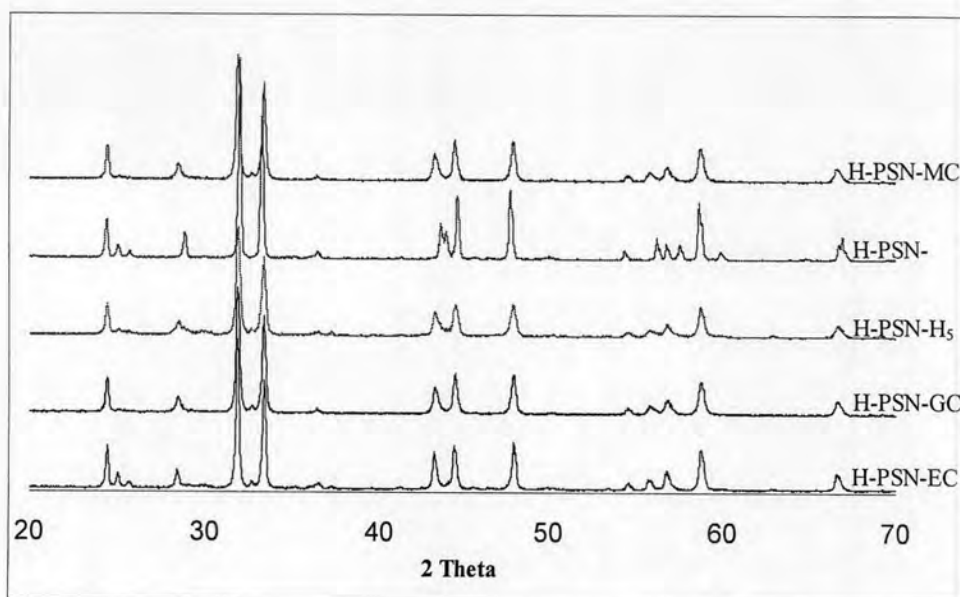


Figure 3.6 The XRD patterns of PrSrNiO₄ powders synthesized by hydrothermal method using various chelating agents.

Table 3.7 Crystallite sizes of synthesized PSN powders by hydrothermal method using different chelating agents

Perovskites	Crytrallite size (nm)
H-PSN-MC	32
H-PSN-G	30
H-PSN-H ₅	37
H-PSN-GC	33
H-PSN-EC	31

The slightly dcreased of crystallite size of these oxides was observed for the PSN acquired by hydrothermal method when compared with sol gel method. In addition, glycine still exhibited the smallest crystallite sizes of 30 nm.

For ABO_3 structure, crystallite size decreased when hydrothermal method was applied. On the contrary, K_2NiF_4 structure, crystallite size decreased slightly when hydrothermal approach was used.

The complex oxides $La_{0.7}Sr_{0.3}Ga_{0.7}Fe_{0.2}Mg_{0.1}O_{3-\delta}$ and $La_{0.8}Sr_{0.2}Ga_{0.8}Mg_{0.15}Co_{0.05}O_{3-\delta}$ prepared by conventional solid-state reaction method were reported [30-31]. The starting materials were metal oxides. In this research, $La_{0.7}Sr_{0.3}Ga_{0.7}Fe_{0.2}Mg_{0.1}O_{3-\delta}$ and $La_{0.8}Sr_{0.2}Ga_{0.8}Mg_{0.15}Co_{0.05}O_{3-\delta}$ were attempted to synthesize by using metal nitrates both sol gel and hydrothermal methods to reduce the cost of expensive metal oxides. The preparations of both oxides by only hydrothermal method were successful. The complete structure of LSGFM and LSGCM were formed after sintering.

3.2.1.7 Phase formation of $La_{0.7}Sr_{0.3}Ga_{0.7}Fe_{0.2}Mg_{0.1}O_3$ (synthesized by hydrothermal method)

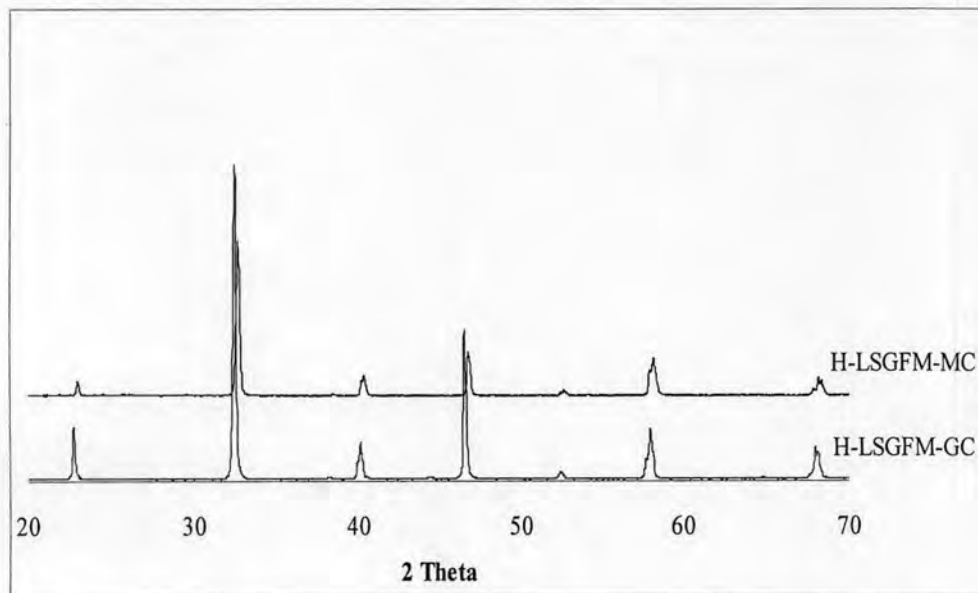


Figure 3.7 The XRD patterns of single phase $La_{0.7}Sr_{0.3}Ga_{0.7}Fe_{0.2}Mg_{0.1}O_{3-\delta}$ sintered disc synthesized by hydrothermal method using various chelating agents after sintered at $1450^{\circ}C$ for 10 hours.

Figure 3.7 shows XRD patterns of $La_{0.7}Sr_{0.3}Ga_{0.7}Fe_{0.2}Mg_{0.1}O_{3-\delta}$ with single phase of ABO_3 structure. It was found that the perovskite oxides prepared using

citric acid and glycine-citric acid as chelating agents showed the single phase and cubic structure. It is mentioned that $\text{La}_{0.7}\text{Sr}_{0.3}\text{Ga}_{0.7}\text{Fe}_{0.2}\text{Mg}_{0.1}\text{O}_{3-\delta}$ was prepared by hydrothermal method using starting materials as metal nitrates.

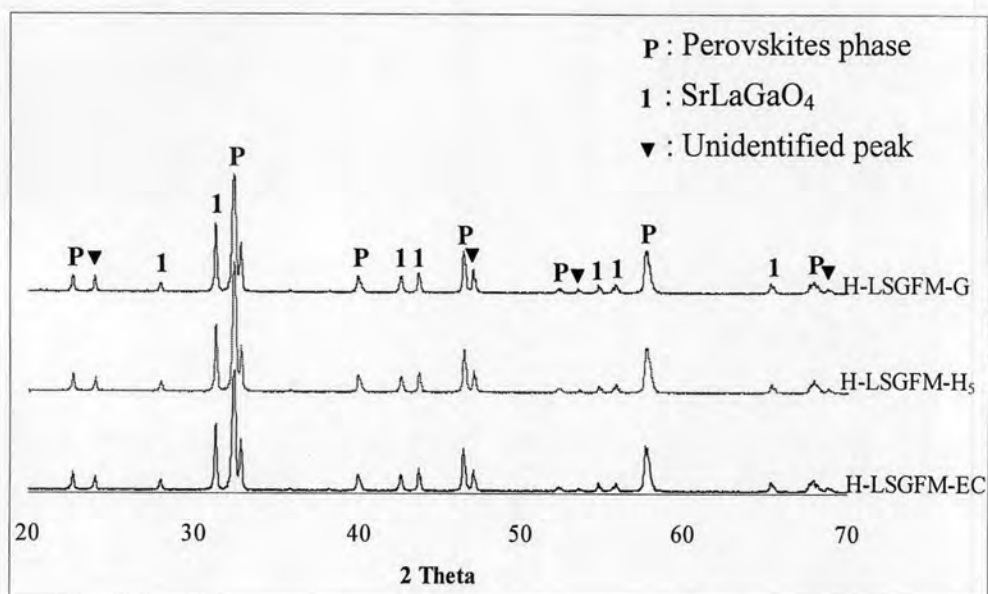


Figure 3.8 The XRD patterns of $\text{La}_{0.7}\text{Sr}_{0.3}\text{Ga}_{0.7}\text{Fe}_{0.2}\text{Mg}_{0.1}\text{O}_{3-\delta}$ sintered disc synthesized by hydrothermal method with using various chelating agents after sintered at 1450°C for 10 hours.

XRD peaks of H-LSGFM-G, H-LSGFM-H₅ and H-LSGFM-EC show the SrLaGaO_4 and unidentified peaks along the perovskite phase.

3.2.1.8 Phase formation of $\text{La}_{0.8}\text{Sr}_{0.2}\text{Ga}_{0.8}\text{Mg}_{0.15}\text{Co}_{0.05}\text{O}_{3-\delta}$ (synthesized by hydrothermal method)

$\text{La}_{0.8}\text{Sr}_{0.2}\text{Ga}_{0.8}\text{Mg}_{0.15}\text{Co}_{0.05}\text{O}_{3-\delta}$ single phase was formed when hydrothermal method was applied (Figure 3.9). And citric acid was used as chelating ligand. It is indicated that citric acid can chelate metal cations under ambient condition.

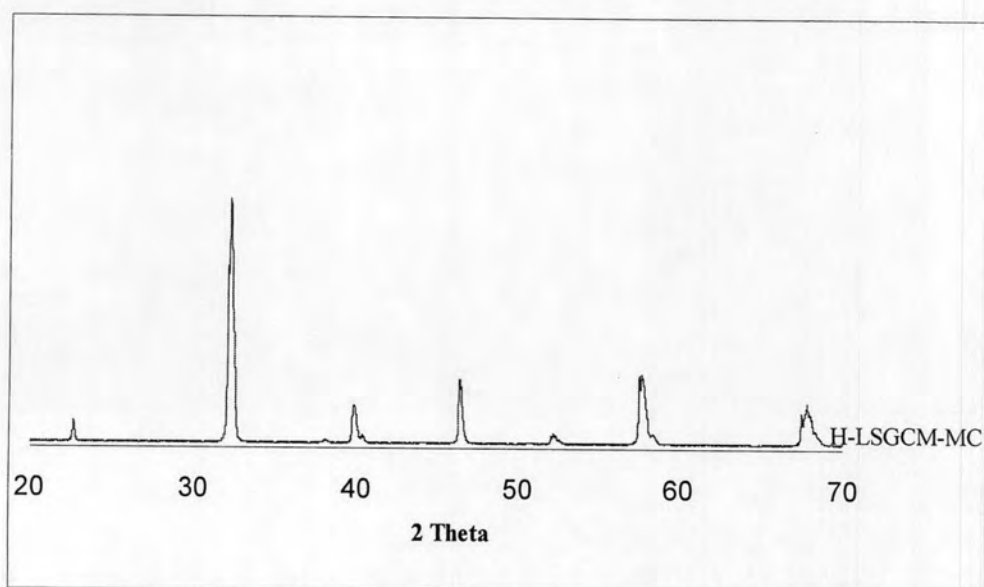


Figure 3.9 The XRD patterns of single phase $\text{La}_{0.8}\text{Sr}_{0.2}\text{Ga}_{0.8}\text{Mg}_{0.15}\text{Co}_{0.05}\text{O}_{3-\delta}$ sintered disc synthesized by hydrothermal method using various chelating agents after sintered at 1450°C for 10 hours.

On the contrary, perovskites oxide synthesized by using chelating agents such as G, H_5DTPA , GC and EC did not exhibit the single phase of $\text{La}_{0.8}\text{Sr}_{0.2}\text{Ga}_{0.8}\text{Mg}_{0.15}\text{Co}_{0.05}\text{O}_{3-\delta}$. The secondary phase as SrLaGaO_4 and unidentified phase appeared (Figure 3.10).

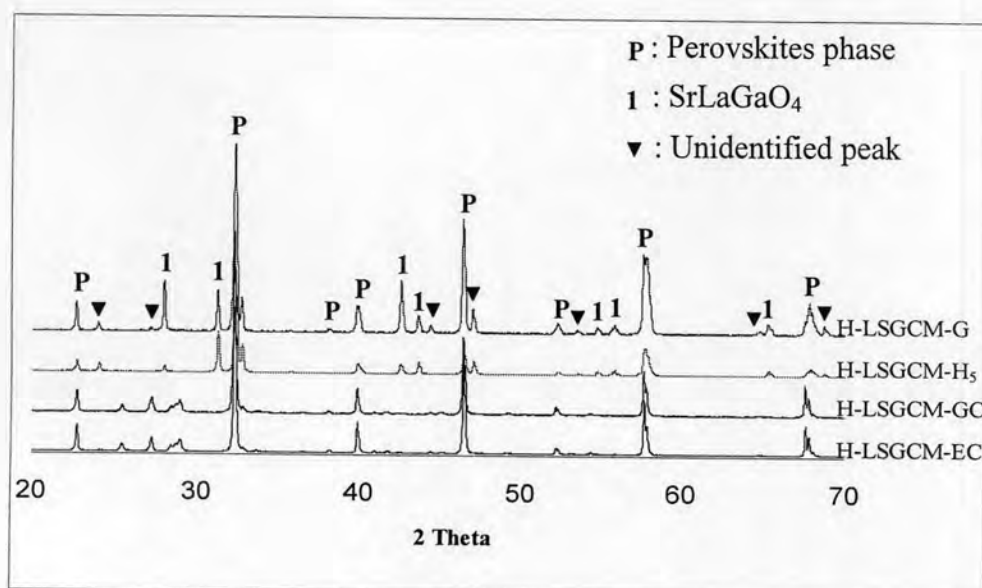


Figure 3.10 The XRD patterns of $\text{La}_{0.8}\text{Sr}_{0.2}\text{Ga}_{0.8}\text{Mg}_{0.15}\text{Co}_{0.05}\text{O}_{3-\delta}$ sintered disc synthesized by hydrothermal method using various chelating agents after sintered at 1450°C for 10 hours.

This work indicated that hydrothermal method was bear on crystallite formation. Therefore, precursor that achieved from hydrothermal method was facility to combustion thus the crystallite size was small due to the reduction temperature and time for ignition auto combustion. Namely, the chemical composition of the powders can be easily controlled from the perspective of stoichiometry and formation of solid solutions.

3.2.2 Scanning electron microscope (SEM) and density

The morphologies of perovskite particles and sintered disc were examined by SEM technique. The particle sizes were obtained by measuring the particles in SEM images by SEMAFORE V.5 software. The particle sizes of these oxides were compared. Densities of samples were determined by the Archimedes immersion method using water as a medium.

3.2.2.1 The morphology of $\text{Ba}_{0.5}\text{Sr}_{0.5}\text{Co}_{0.8}\text{Fe}_{0.2}\text{O}_{3-\delta}$ particles (synthesized by sol gel method)

Figure 3.11 shows different particles morphologies of BSCF powders synthesized by various chelating agents. The SEM micrograph of S-BSCF-MC exhibited the fine particles and tiny agglomeration. More agglomeration was observed in S-BSCF-G, S-BSCF-EC and S-BSCF-GC, Finally, the massive agglomeration was observed in S-BSCF-H₅. From the reason, the energy released during the combustion should be enough to form oxide powders, but not excessive to avoid the agglomeration of the particles [29]. Hence MC, G, GC, and EC combustion is capable of producing BSCF powders despite the short duration of auto-ignition. Therefore the S-BSCF-H₅ exhibited the largest particles size (~2.103 μm) as shown in Table 3.8.

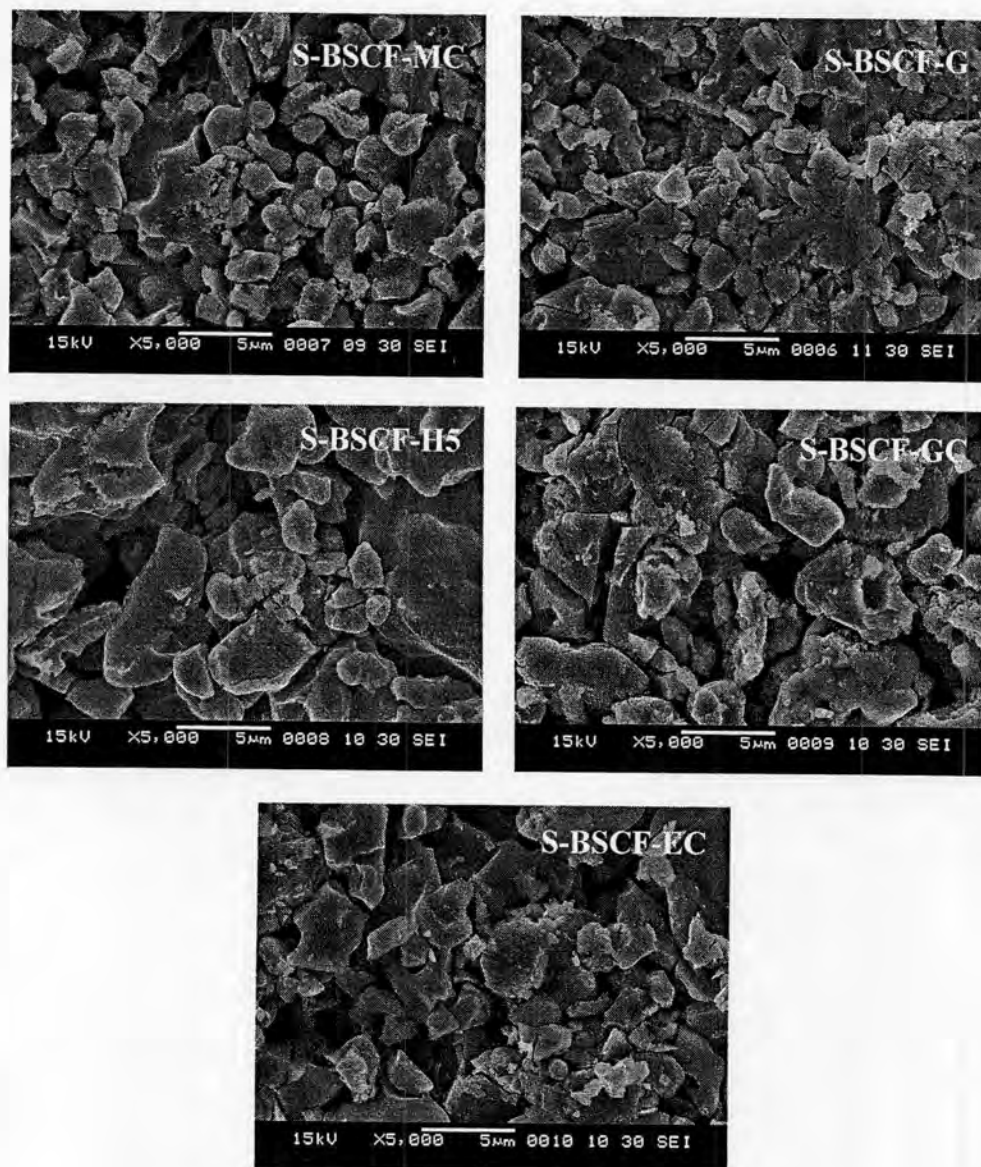


Figure 3.11 Surface morphology of $\text{Ba}_{0.5}\text{Sr}_{0.5}\text{Co}_{0.8}\text{Fe}_{0.2}\text{O}_{3-\delta}$ particles synthesized by sol gel method using various chelating agents after calcined at 900°C for 6 hours.

Table 3.8 Particle sizes of synthesized $\text{Ba}_{0.5}\text{Sr}_{0.5}\text{Co}_{0.8}\text{Fe}_{0.2}\text{O}_{3-\delta}$ powders by sol gel method with using different chelating agents

Perovskites	Particles size (μm)
S-BSCF-MC	0.897
S-BSCF-G	1.152
S-BSCF-H ₅	2.103
S-BSCF-GC	1.282
S-BSCF-EC	1.242

3.2.2.2 The morphology of $\text{Ba}_{0.5}\text{Sr}_{0.5}\text{Co}_{0.8}\text{Fe}_{0.2}\text{O}_{3-\delta}$ particles (synthesized by hydrothermal method)

Figure 3.12 and Table 3.9 show the morphologies and particles size of samples synthesized by hydrothermal method using various chelating agents. The resulting in a drastic decreased in particles size and aggregation of particles when it was compared with sol gel method. Moreover, the morphologies of these were homogeneous and spherical than the powders synthesized by sol gel method. As mentioned before, hydrothermal method had ability to control of size and morphology of crystallites and significantly reduced aggregation levels. In case of using EC, citric acid was used to chelate metal ions, ethylene glycol serves as a solvent for the process of polymerization between citric acid and ethylene glycol. Esterification takes place by attachment of one of the end hydroxyl groups of ethylene glycol to the end carboxyl group of metal citrate while releasing a water molecule. The ambient conditions of hydrothermal method enhances the polyesterification process by facilitating attachment of several metal citrates' carboxyl groups together with the remaining hydroxyl groups of ethylene glycols. Thus, H-BSCF-EC showed the smallest particles size of 0.404 μm .

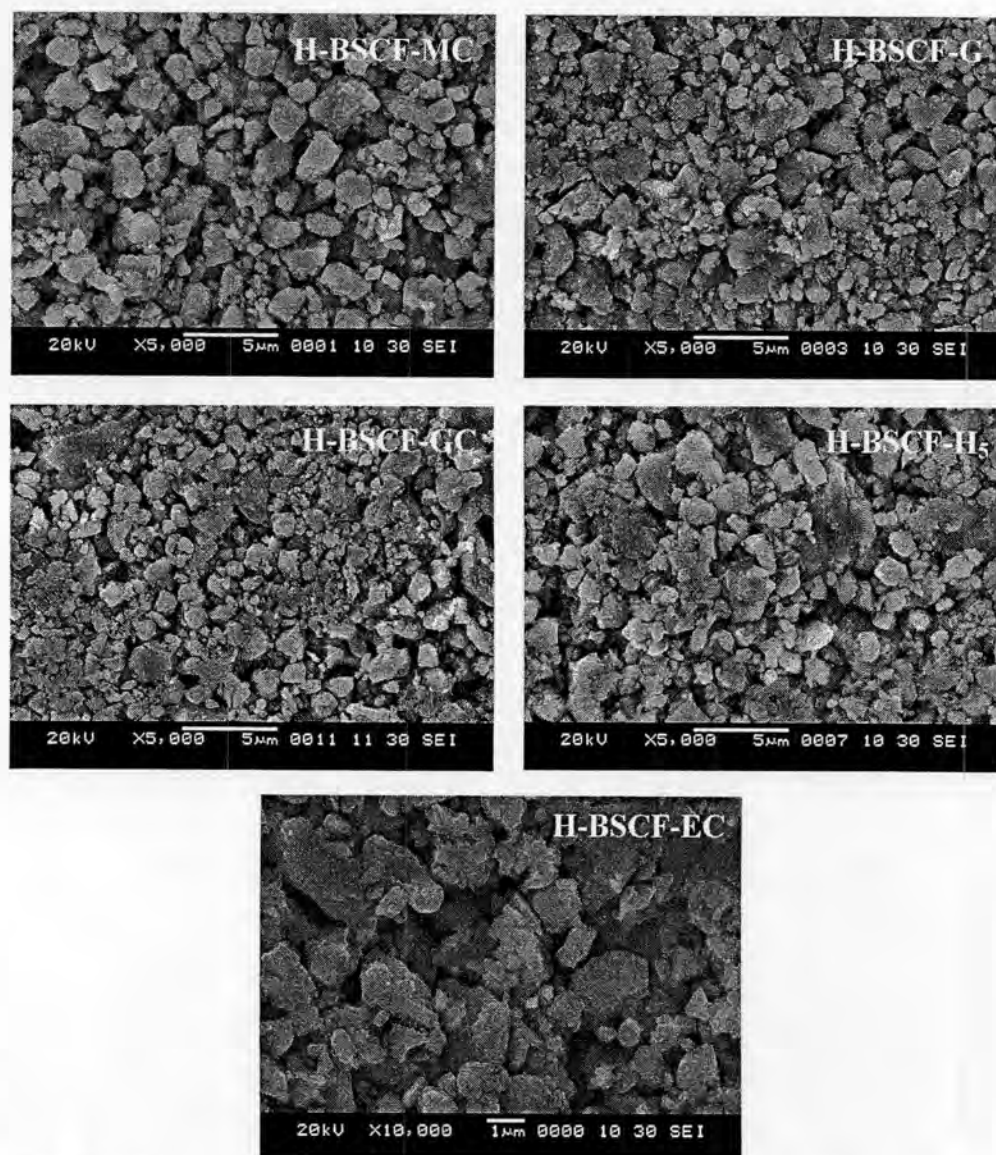


Figure 3.12 Surface morphology of $\text{Ba}_{0.5}\text{Sr}_{0.5}\text{Co}_{0.8}\text{Fe}_{0.2}\text{O}_{3-\delta}$ particles synthesized by hydrothermal method using various chelating agents after calcined at 900°C for 6 hours.

Table 3.9 Particle sizes of synthesized $\text{Ba}_{0.5}\text{Sr}_{0.5}\text{Co}_{0.8}\text{Fe}_{0.2}\text{O}_{3-\delta}$ powders by sol gel and hydrothermal method using different chelating agents

Perovskites	Particle sizes (μm)	
	Sol gel method	Hydrothermal method
BSCF-MC	0.897	0.679
BSCF-G	1.152	0.858
BSCF- H_5	2.103	0.564
BSCF-GC	1.282	0.734
BSCF-EC	1.242	0.404

3.2.2.3 The morphology of $\text{Ba}_{0.5}\text{Sr}_{0.5}\text{Co}_{0.8}\text{Fe}_{0.2}\text{O}_{3-\delta}$ sintered disc (synthesized by sol gel method)

The morphologies of BSCF synthesized by sol gel method using different chelating agents were presented in Figure 3.13. As the results, S-BSCF-G specimen had impurity on the surface and all of specimens had many pore. It was found that sintered disc synthesized by using H_5DTPA had the smallest grains size ($\sim 13.229 \mu\text{m}$). Contrast with particles size that powders synthesized by using H_5DTPA show the largest size. Therefore disc synthesized by using glycine-citrate show the largest size ($\sim 17.283 \mu\text{m}$).

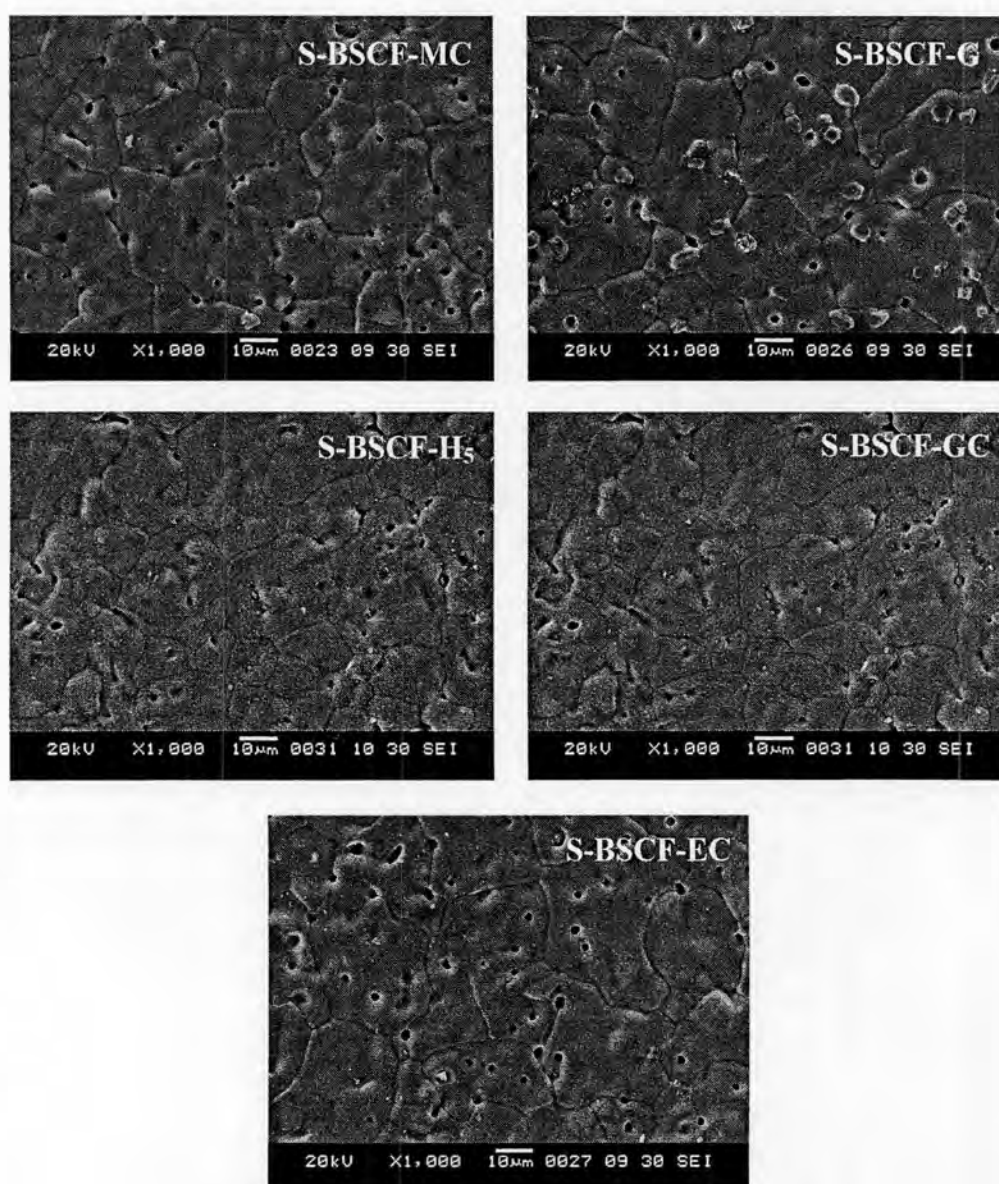


Figure 3.13 Surface morphology of $\text{Ba}_{0.5}\text{Sr}_{0.5}\text{Co}_{0.8}\text{Fe}_{0.2}\text{O}_{3-\delta}$ sintered disc synthesized by sol gel method using various chelating agents after sintered at 1100°C for 10 hours.

The densities of $\text{Ba}_{0.5}\text{Sr}_{0.5}\text{Co}_{0.8}\text{Fe}_{0.2}\text{O}_{3-\delta}$ obtained from various chelating agents were listed in Table 3.10.

Table 3.10 Density of $\text{Ba}_{0.5}\text{Sr}_{0.5}\text{Co}_{0.8}\text{Fe}_{0.2}\text{O}_{3-\delta}$ discs synthesized by sol gel method using different chelating agents

Perovskites	Density (g.cm^3)
S-BSCF-MC	5.310
S-BSCF-G	5.332
S-BSCF-H ₅	5.468
S-BSCF-GC	5.381
S-BSCF-EC	5.524

3.2.2.4 The morphology of $\text{Ba}_{0.5}\text{Sr}_{0.5}\text{Co}_{0.8}\text{Fe}_{0.2}\text{O}_{3-\delta}$ grains (synthesized by hydrothermal method)

Figure 3.14 shows SEM micrograph of $\text{Ba}_{0.5}\text{Sr}_{0.5}\text{Co}_{0.8}\text{Fe}_{0.2}\text{O}_{3-\delta}$ disc synthesized by hydrothermal method. It was found that BSCF prepared by using H₅DTPA had an impurity on the surface. Moreover, the specimens prepared by hydrothermal method had a lot of pore than that those by sol gel method (Figure 3.11). As the reason of, the powders obtained from hydrothermal method were smaller than sol gel method. Thus, it will be fused together easier than that one.

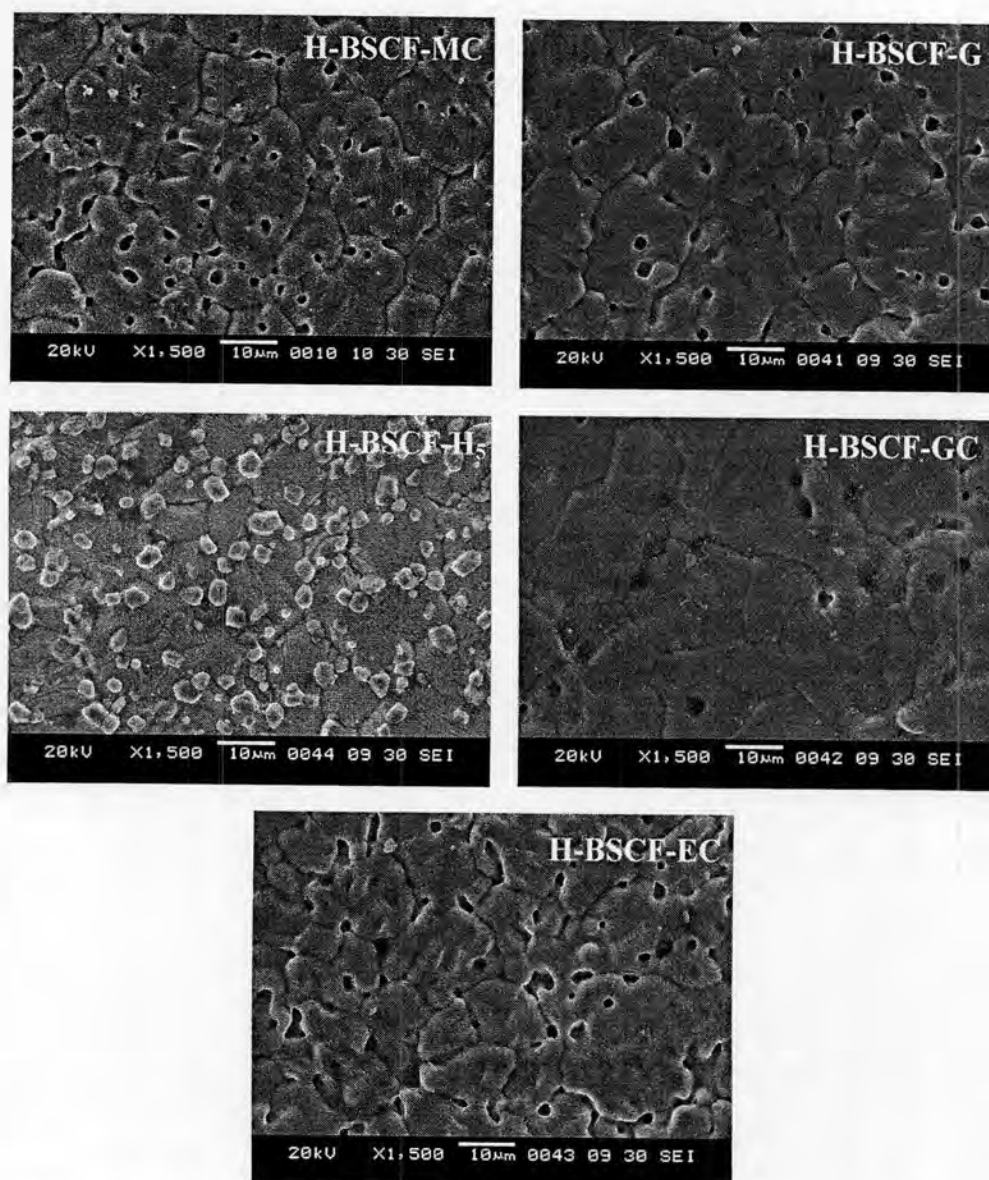


Figure 3.14 Surface morphology of $\text{Ba}_{0.5}\text{Sr}_{0.5}\text{Co}_{0.8}\text{Fe}_{0.2}\text{O}_{3-\delta}$ sintered disc synthesized by hydrothermal method using various chelating agents after sintered at 1100°C for 10 hours.

The densities of $\text{Ba}_{0.5}\text{Sr}_{0.5}\text{Co}_{0.8}\text{Fe}_{0.2}\text{O}_{3-\delta}$ discs with various chelating agents were listed in Table 3.11. It is confirmed by SEM results that there were a lot of pore on the surface of the specimens disc. Because the same sintering temperature, smaller particle size can be fused easily than the larger. Therefore the density of hydrothermal method will be small.

Table 3.11 Density of $Ba_{0.5}Sr_{0.5}Co_{0.8}Fe_{0.2}O_{3-\delta}$ discs synthesized by hydrothermal method with using different chelating agents

Perovskites	Density (g.cm ³)
H-BSCF-MC	5.195
H-BSCF-G	5.226
H-BSCF-H ₅	5.471
H-BSCF-GC	4.460
H-BSCF-EC	4.657

3.2.2.5 The morphology of $PrSrCoO_4$ particles (synthesized by sol gel method)

The morphologies of PSC particles synthesized by sol gel method were spherical as presented in Figure 3.15. As the result, PSC particles obtained by using MC, GC and EC as a chelating agent were homogeneous, small and tiny agglomeration than that those from by using H₅DTPA and G. It can be explained that glycine had one carboxylic group thus; chelating ability of glycine was a little. The amount of carbonyl acid group (COOH) plays an important role in keeping the homogeneity of precursor. To prevent the precipitation occurring over the whole concentration process and to maintain the homogeneity of the metal ions in the resin on a molecular scale, the molar ratio of chelating agents to metal ions should be high enough [32]. In case of glycine, some precipitation occurred, affecting the homogeneity of the final products. On the other hand, H₅DTPA, as mentioned earlier that the excessive energy released during combustion contributed to the agglomeration of the particles.

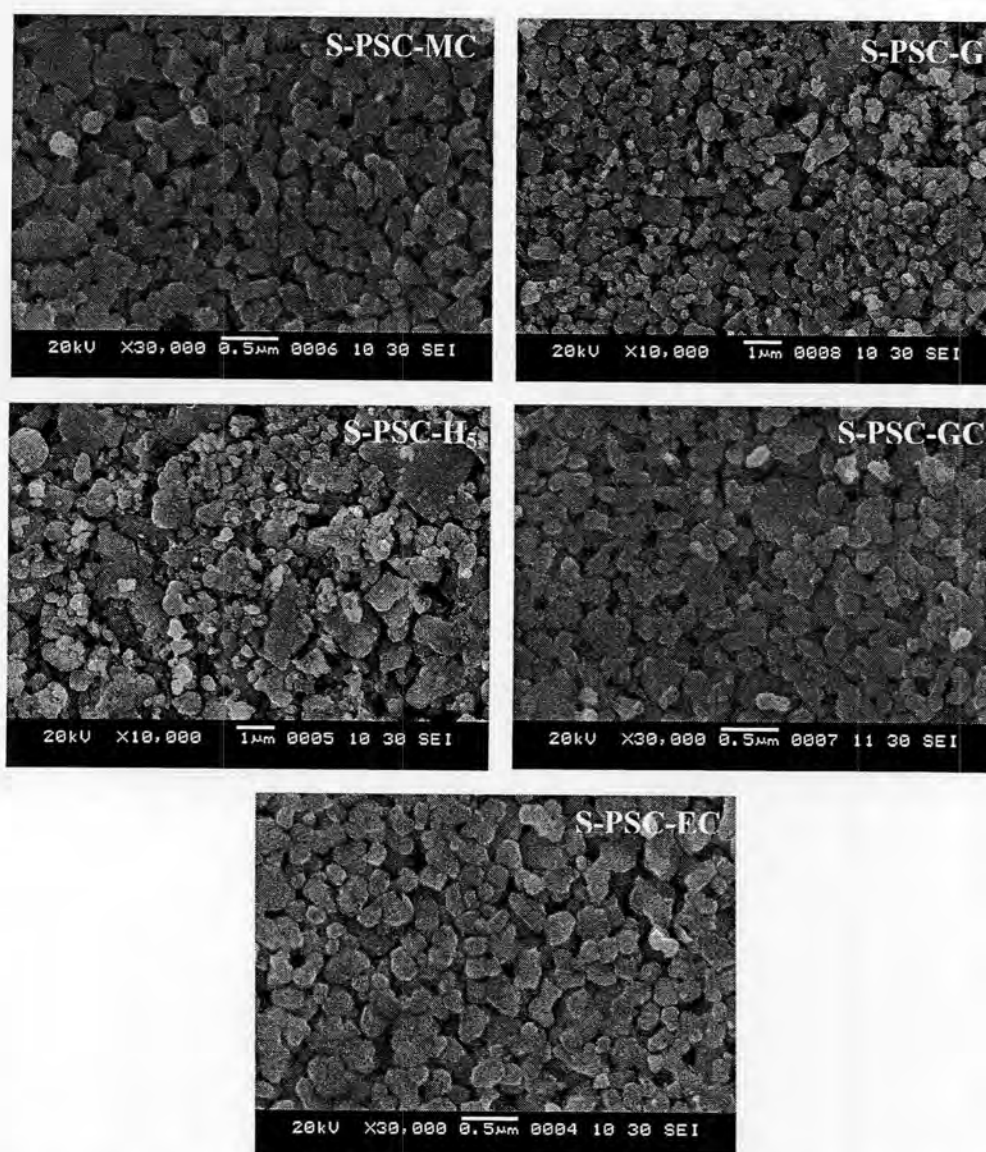


Figure 3.15 Surface morphology of PrSrCoO₄ particles synthesized by sol gel method using various chelating agents after calcined at 900°C for 6 hours.

Table 3.12 Particle sizes of synthesized PrSrCoO₄ powders by sol gel method with using different chelating agents

Perovskites	Particles size (μm)
S-PSC-MC	0.209
S-PSC-G	0.358
S-PSC-H ₅	0.495
S-PSC-GC	0.180
S-PSC-EC	0.202

3.2.2.6 The morphology of PrSrCoO_4 particles (synthesized by hydrothermal method)

SEM pictures of PSC particles synthesized by hydrothermal method show homogeneous spherical particles (Figure 3.16). It is shown that the particle sizes of H_5DTPA was extremely decreased from 0.495 to 0.190 μm using hydrothermal method.

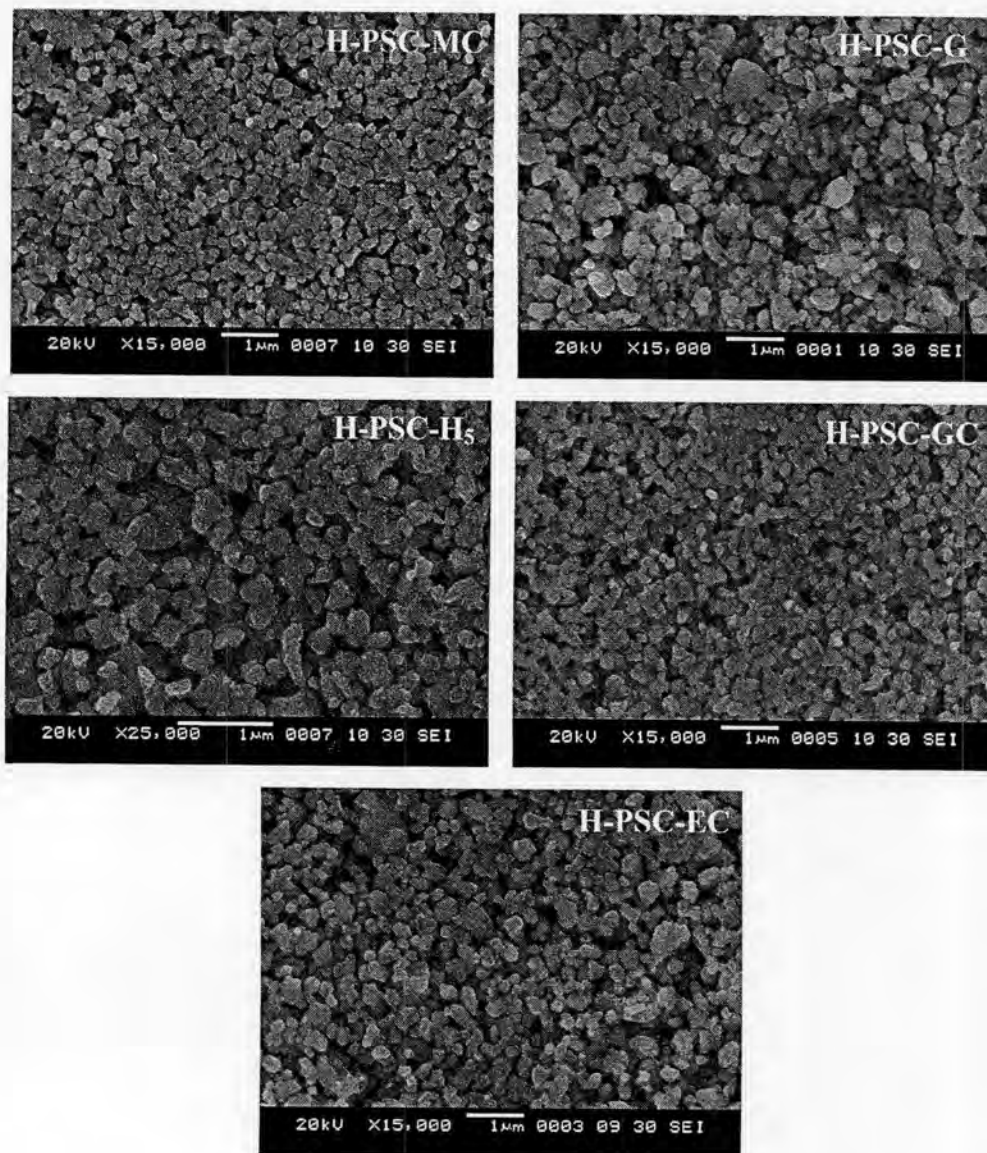


Figure 3.16 Surface morphology of PrSrCoO_4 particles synthesized by hydrothermal method using various chelating agents after calcined at 900°C for 6 hours.

Table 3.13 Particle sizes of synthesized PrSrCoO₄ powders by sol gel and hydrothermal method with using different chelating agents

Perovskites	Particles size (μm)	
	Sol gel method	Hydrothermal method
PSC-MC	0.209	0.227
PSC-G	0.358	0.235
PSC-H ₅	0.495	0.190
PSC-GC	0.180	0.199
PSC-EC	0.202	0.268

3.2.2.7 The morphology of PrSrCoO₄ sintered disc (synthesized by hydrothermal method)

The sintered disc showed crack-free and no porosity. The H-PSC-EC exhibited the dense disc and largest grain size. The others also showed dense packing grain in the size range of 1–2.4 μm.

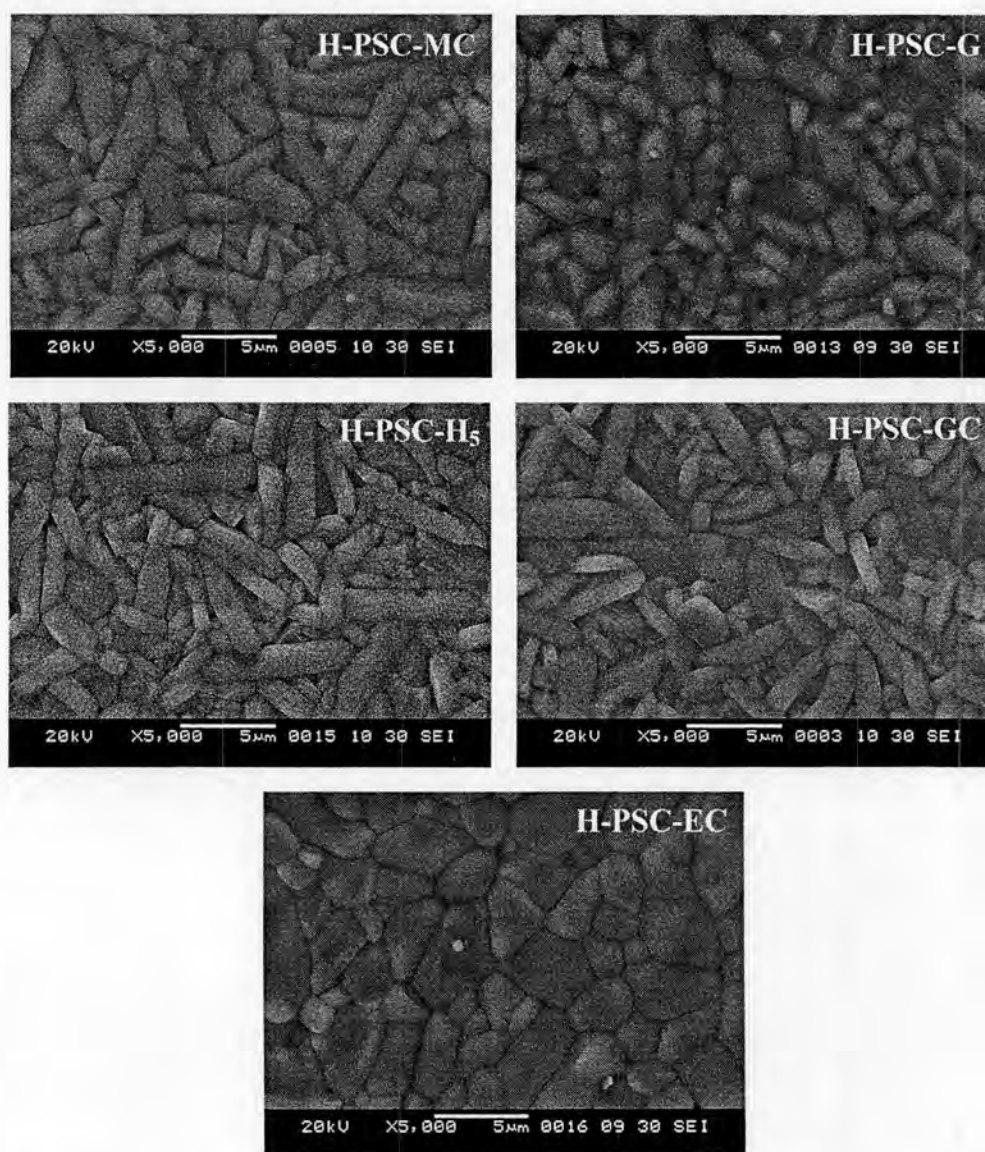


Figure 3.17 Surface morphology of PrSrCoO_4 sintered disc synthesized by hydrothermal method using various chelating agents after sintered at 1200°C for 10 hours.

Density of PSC were listed in Table 3.17, it revealed that chelating agent had slightly effect on the density of sintered disc, H-PSC-EC showed the highest density of 6.617 g.cm^3 .

Table 3.14 Density of PrSrCoO₄ disc synthesized by hydrothermal method with using different chelating agents

Perovskites	Density (g.cm ³)
H-PSC-MC	6.391
H-PSC-G	6.157
H-PSC-H ₅	6.177
H-PSC-GC	6.439
H-PSC-EC	6.617

3.2.2.8 The morphology of PrSrNiO₄ particles (synthesized by sol gel method)

Figure 3.18 shows the sphere of PSN particles synthesized by sol gel method. SEM micrograph of S-PSN-H₅ and S-PSN-EC showed the agglomeration of the fine particles, lead to the bigger particles. S-PSN-MC exhibited the smallest particles size of 0.131 μm (Table 3.15).

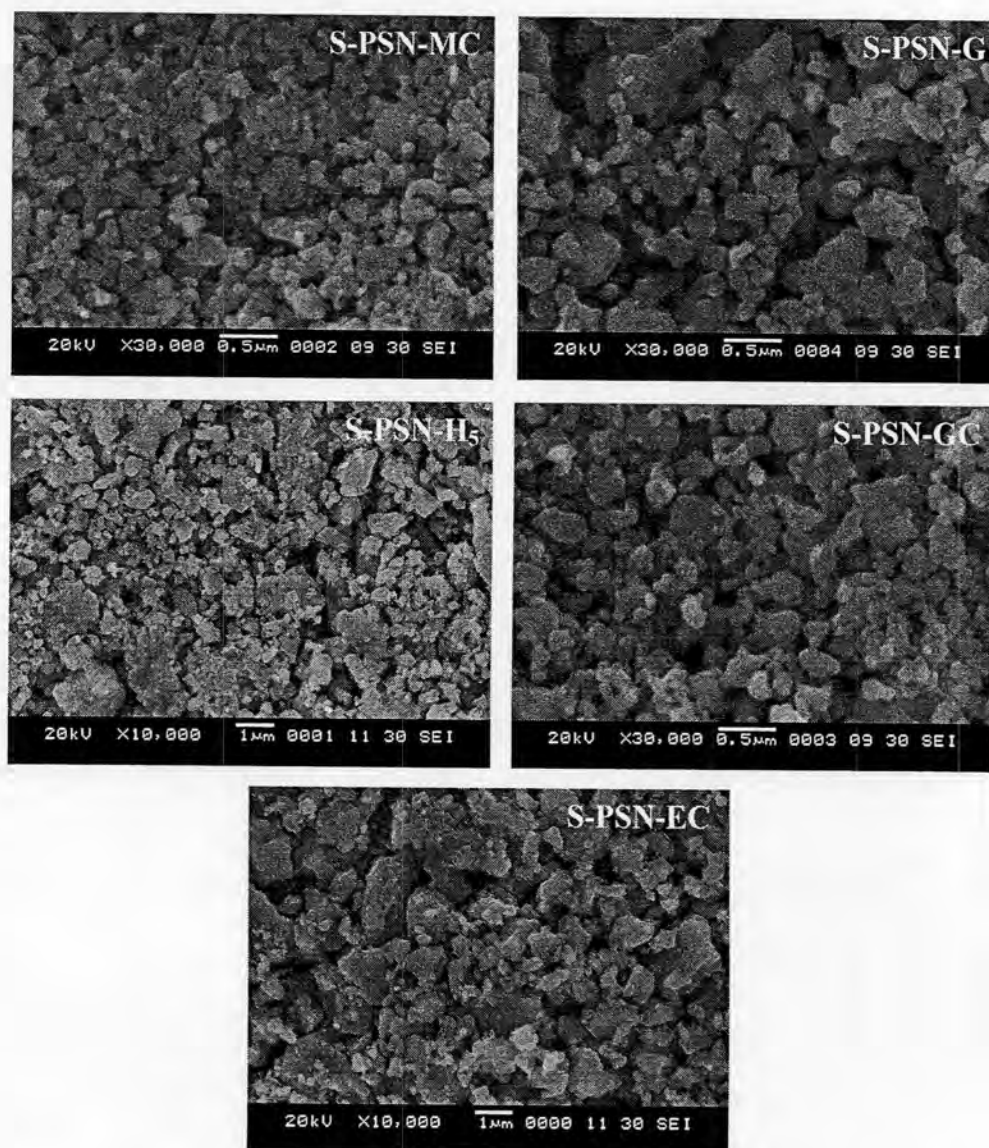


Figure 3.18 Surface morphology of PrSrNiO_4 particles synthesized by sol gel method using various chelating agents after calcined at 900°C for 6 hours.

Table 3.15 Particle sizes of synthesized PrSrNiO_4 powders by sol gel method with using different chelating agents

Perovskites	Particles size (μm)
S-PSN-MC	0.131
S-PSN-G	0.186
S-PSN- H_5	0.337
S-PSN-GC	0.163
S-PSN-EC	0.499

3.2.2.9 The morphology of PrSrNiO₄ particles (synthesized by hydrothermal method)

PSN particle sizes prepared by hydrothermal method were decreased as compared with sol gel method. Moreover, the particles size of H-PSN-H₅ and H-PSN-EC was extremely decreased. It is indicated that hydrothermal temperature ambient condition enhances the chelating ability of H₅DTPA with metal ions and enhances the polyesterification process of EC. However, H-PSN-MC particle size was slightly increased to 0.150 μm (Table 3.16).

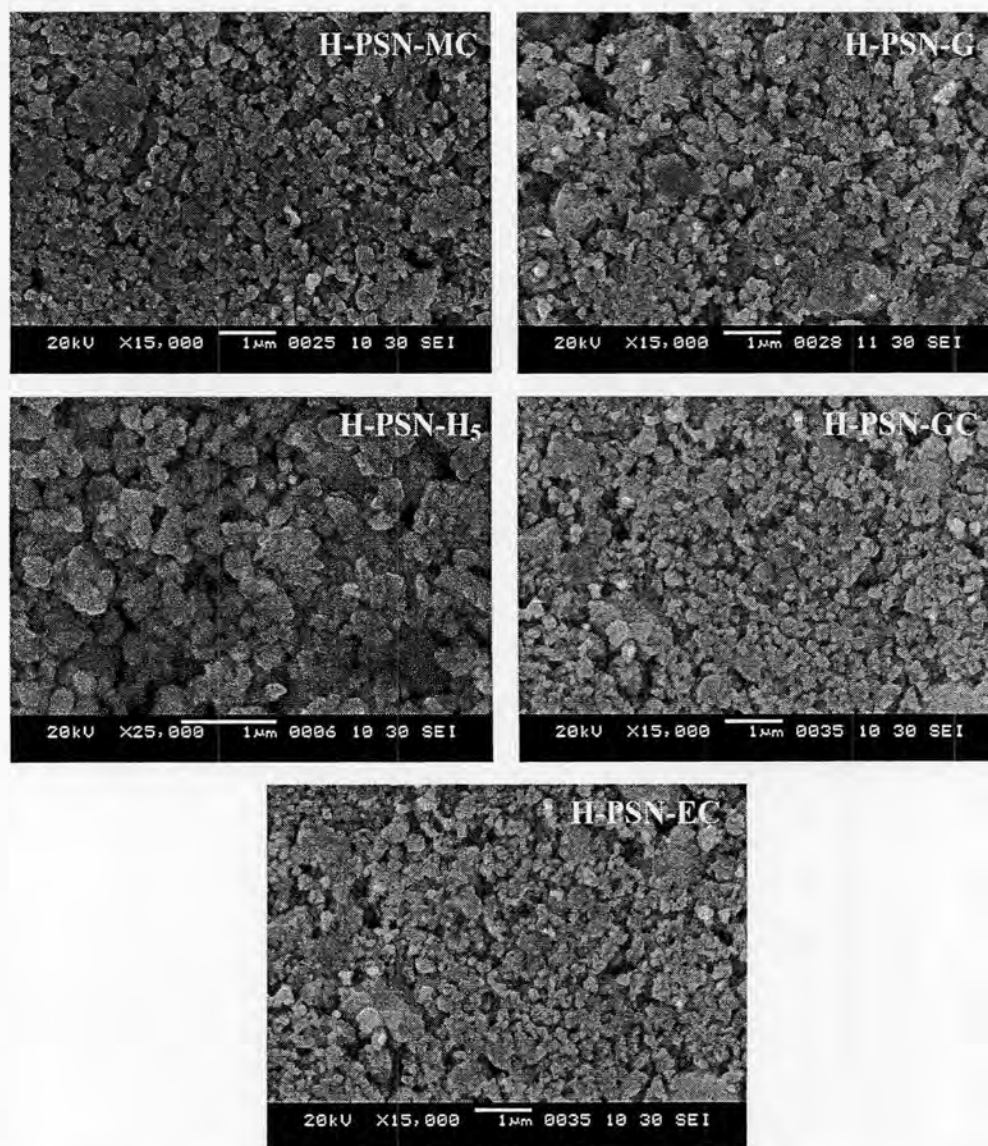


Figure 3.19 Surface morphology of PrSrNiO₄ particles synthesized by hydrothermal method using various chelating agents after calcined at 900°C for 6 hours.

Table 3.16 Particle sizes of synthesized PrSrNiO₄ powders by sol gel method compared with hydrothermal method

Perovskites	Particles size (μm)	
	Sol gel method	Hydrothermal method
PSN-MC	0.131	0.150
PSN-G	0.186	0.182
PSN-H ₅	0.337	0.185
PSN-GC	0.163	0.139
PSN-EC	0.499	0.142

3.2.2.10 The morphology of PrSrNiO₄ sintered disc (synthesized by hydrothermal method)

SEM observations of PSN prepared by hydrothermal method proved that all of chelating agents had slightly effected to the grains size formation. All of PSN grain sizes were small sphere but had many pores. The H-PSN-MC specimen had the most porosity which confirmed by the lowest density in Table 3.20. In contrast of H-PSN-GC showed the dense packed grain.

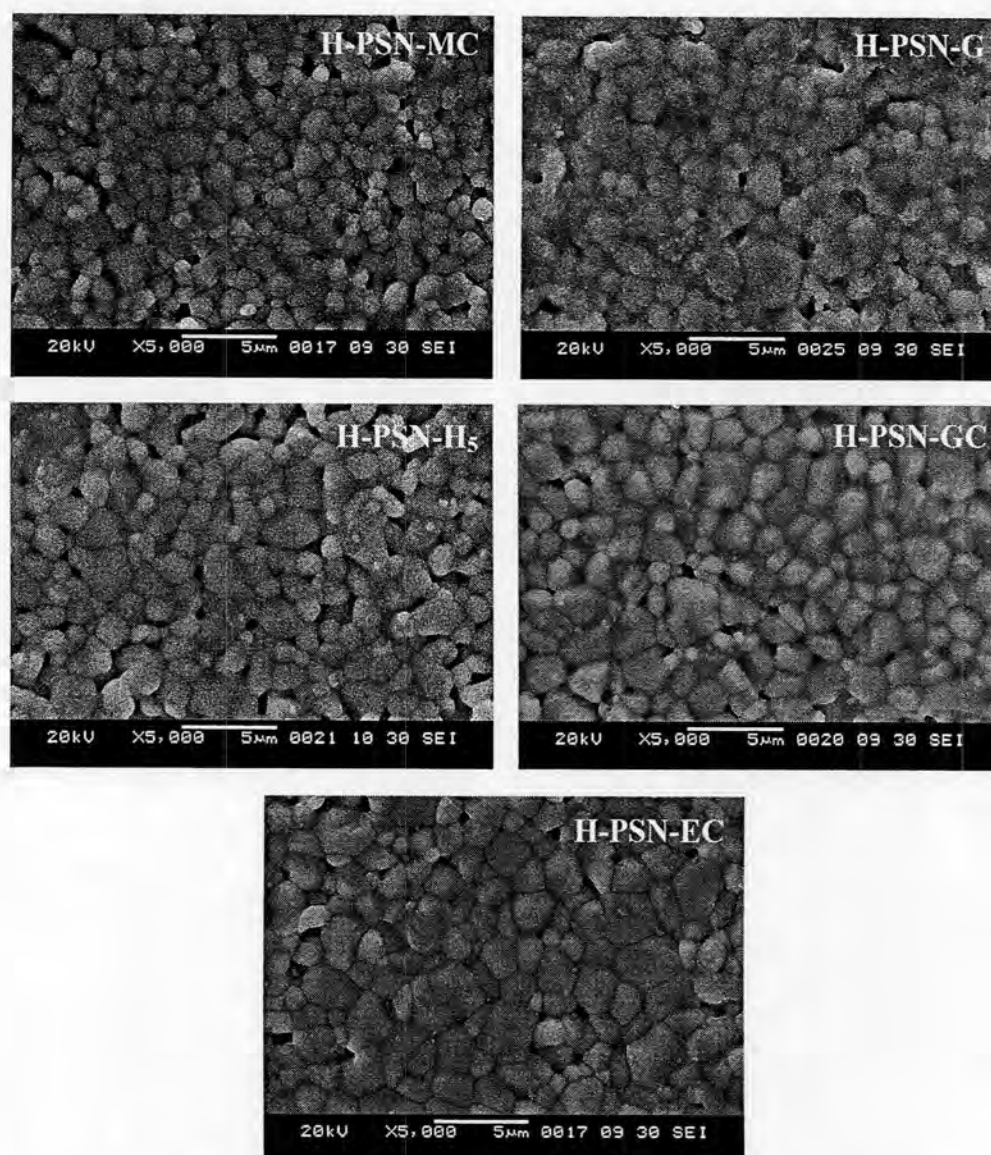


Figure 3.20 Surface morphology of PrSrNiO_4 sintered disc synthesized by hydrothermal method using various chelating agents after sintered at 1200°C for 10 hours.

Table 3.17 Density of PrSrNiO₄ discs synthesized by hydrothermal method using different chelating agents

Perovskites	Density (g.cm ³)
H-PSN-MC	4.991
H-PSN-G	5.226
H-PSN-H ₅	5.075
H-PSN-GC	5.442
H-PSN-EC	5.200

For La_{0.7}Sr_{0.3}Ga_{0.7}Fe_{0.2}Mg_{0.1}O_{3-δ} and La_{0.8}Sr_{0.2}Ga_{0.8}Mg_{0.15}Co_{0.05}O_{3-δ} the single phase can not be obtained after calcined. The complete structure of ABO₃ occurred after sintering.

3.2.2.11 The morphology of La_{0.7}Sr_{0.3}Ga_{0.7}Fe_{0.2}Mg_{0.1}O_{3-δ} sintered disc (synthesized by hydrothermal method)

Figure 3.21 showed the morphology of LSGFM discs. H-LSGFM-MC showed more homogeneous and smaller grain than H-LSGFM-GC.

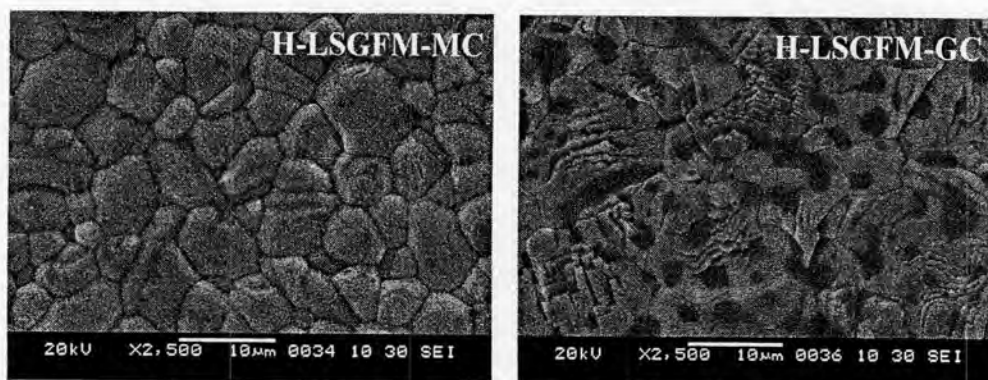


Figure 3.21 Surface morphology of La_{0.7}Sr_{0.3}Ga_{0.7}Fe_{0.2}Mg_{0.1}O_{3-δ} sintered disc synthesized by hydrothermal method using citric acid and glycine-citrate as chelating agents after sintered at 1450°C for 10 hours.

The density was listed in Table 3.18. It was shown that H-LSGFM-GC had higher density than H-LSGFM-MC.

Table 3.18 Density of $\text{La}_{0.7}\text{Sr}_{0.3}\text{Ga}_{0.7}\text{Fe}_{0.2}\text{Mg}_{0.1}\text{O}_{3-\delta}$ discs synthesized by hydrothermal method with using different chelating agents

Perovskites	Density (g.cm^3)
H-LSGFM-MC	5.578
H-LSGFM-GC	6.984

3.2.2.12 The morphology of $\text{La}_{0.8}\text{Sr}_{0.2}\text{Ga}_{0.8}\text{Mg}_{0.15}\text{Co}_{0.05}\text{O}_{3-\delta}$ sintered disc (synthesized by hydrothermal method)

LSGCM single phase cannot be obtained after calcination. The sintered disc prepared from using citric acid showed of pure perovskites phase.

$\text{La}_{0.8}\text{Sr}_{0.2}\text{Ga}_{0.8}\text{Mg}_{0.15}\text{Co}_{0.05}\text{O}_{3-\delta}$ showed the large grain size and higher density than $\text{La}_{0.7}\text{Sr}_{0.3}\text{Ga}_{0.7}\text{Fe}_{0.2}\text{Mg}_{0.1}\text{O}_{3-\delta}$ (Figure 3.21 and Table 3.19).

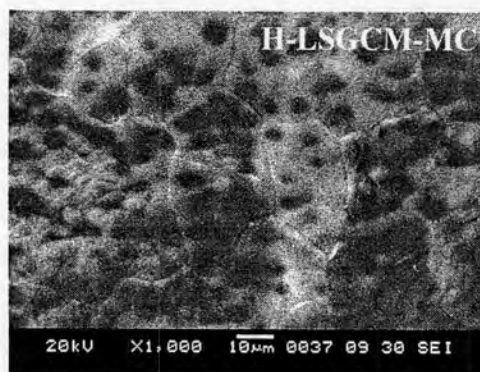


Figure 3.22 Surface morphology of $\text{La}_{0.8}\text{Sr}_{0.2}\text{Ga}_{0.8}\text{Mg}_{0.15}\text{Co}_{0.05}\text{O}_{3-\delta}$ sintered disc synthesized by hydrothermal method using citric acid as chelating agents after sintered at 1450°C for 10 hours.

Table 3.19 Density of $\text{La}_{0.8}\text{Sr}_{0.2}\text{Ga}_{0.8}\text{Mg}_{0.15}\text{Co}_{0.05}\text{O}_{3-\delta}$ discs synthesized by hydrothermal method with using different chelating agents

Perovskites	Density (g.cm^3)
H-LSGCM-MC	6.230

The densities of synthesized perovskites, it was suggested that chelating agent had slightly effected on perovskite discs density. Moreover the densities were high enough for used as materials in SOFC. For BSCF, PSC and PSN, they were used as cathode material. Moreover, LSGFM and LSGCM due to the high density of them thus they were used as electrolyte material.

3.2.3 Electrical conductivity

Generally, there are two kinds of conductive mechanisms (electronic and ionic conductivity) in these MIEC perovskite oxides, owing to the co-presence of holes and oxygen vacancies. As the electronic conductivity is at least one order higher than the ionic conductivity, the measured values (total conductivity) can be mainly referred to the electronic conductivity [33].

In this section, the conductivities of perovskite membranes were studied by DC-4 probe technique in temperature range of 25-800°C due to the operating temperature range of IT-SOFC (600-800°C)

3.2.3.1 Effect of chelating agents on the electrical conductivity of $\text{Ba}_{0.5}\text{Sr}_{0.5}\text{Co}_{0.8}\text{Fe}_{0.2}\text{O}_{3-\delta}$ synthesized by sol gel method

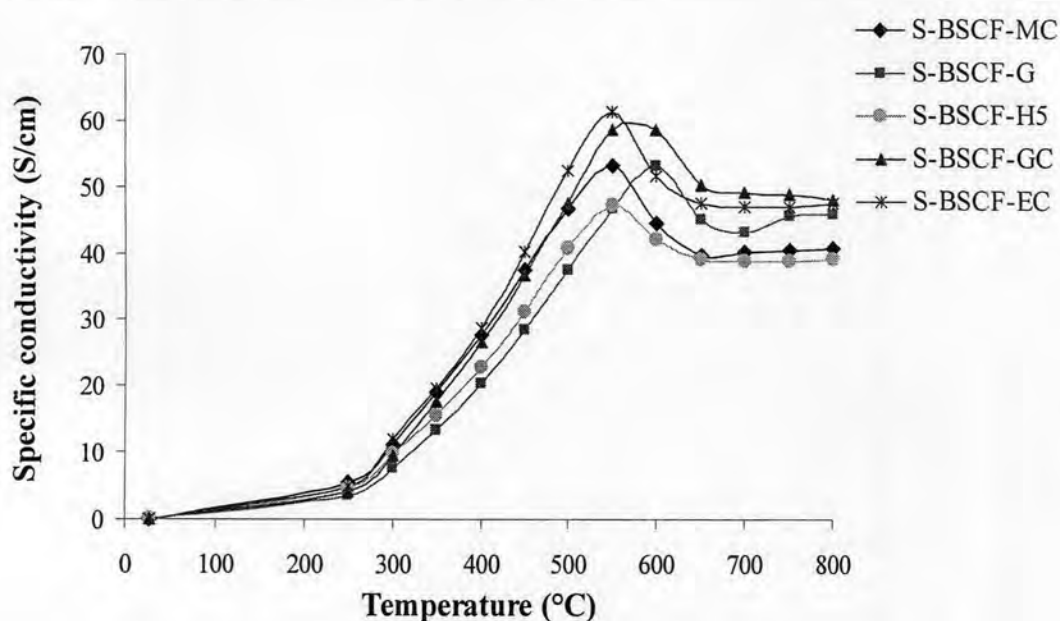
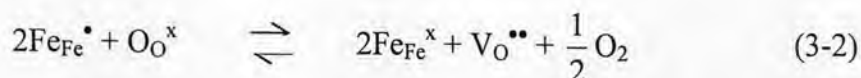
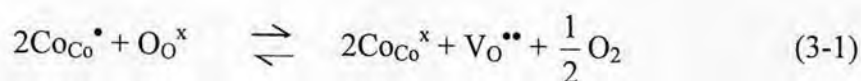


Figure 3.23 Variations of the electrical conductivity measured in air of $\text{Ba}_{0.5}\text{Sr}_{0.5}\text{Co}_{0.8}\text{Fe}_{0.2}\text{O}_{3-\delta}$ synthesized using various chelating agents with temperature.

As presented in Figures 3.23, the electrical conductivity of BSCF synthesized by sol gel method increased gradually with temperature and had the maximum electrical conductivity at 550-600°C. This was due to the behavior of lattice oxygen that became active at this temperature range [34].

The conductivity mechanism can be attributed to two factors. Firstly, the hopping of p-type small polarons were associated with the behavior of triple and tetravalent states of Co and Fe cations. The electron transition between the triple and the tetravalent of Co and Fe caused the electronic conductivity. Secondly, along with the thermal induced lattice oxygen losses, more oxygen deficiency was formed, which thus caused the thermal reduction of Co and Fe cations to lower states as described in equations (3-1) and (3-2) [34].



In Figure 3.23, the electrical conductivity of BSCF synthesized by sol gel method using various chelating agents was measured in air as a function of temperature indicating a semi-conducting behavior at low temperatures ($T \leq 550^{\circ}\text{C}$). The electrical conductivity of each composition increased with temperature up to its maximum value and then decreased. Among all S-BSCFs prepared with different chelating agents, the S-BSCF-EC showed the maximum conductivity (61.2 S/cm) whereas S-BSCF-H₅ exhibited the minimum conductivity (47.2 S/cm) at 550°C. The reasons for the relatively low conductivity of BSCF-H₅ specimens can be mainly interpreted as follow. The total conductivity involves both electronic and ionic conductivity terms due to the presence of holes and oxygen vacancies in the perovskites. In this research, ionic conductivity term had more effect on the total conductivity since the same perovskite was synthesized by using various chelating agents. Thus, there is no significant change in valence state of metal ions in their structures. As a reason, processing conditions may affect the ionic conductivity of perovskite oxides, probably due to an extremely important role of grain boundaries [35]. For perovskite oxide materials current used in intermediate to high temperature electrochemical cells, one of the most important problems is the necessity to decrease grain-

boundary resistivity [36]. In case of S-BSCF-H₅, it exhibited small grains (Figure 3.13) which increased concentration of the grain boundaries and then the conductivity was decreased. Hence, S-BSCF-EC showed moderate grain sizes and highest density (Tables 3.10), leading to the highest conductivity.

Shown in Figure 3.22, the obtained data were presented as Arrhenius plots

$$\sigma = (A/T) \exp(-E_a/RT) \quad (3-3)$$

where A = material constant including the carrier concentration term,

σ = the specific conductivity (S/cm)

E_a = activation energy

R = gas constant

T = temperature (K)

The activation energy (E_a) of S-BSCF specimens that was calculated from the slope of $\log(\sigma \cdot T)$ versus $1000/T$ plots is shown in Table 3.20.

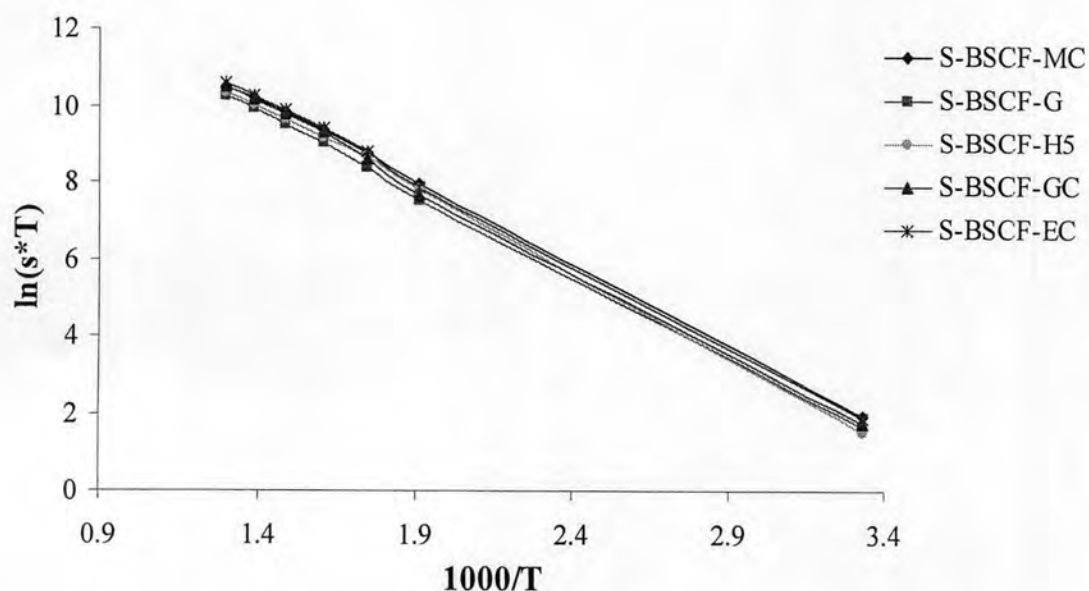


Figure 3.24 Arrhenius plot of $\text{Ba}_{0.5}\text{Sr}_{0.5}\text{Co}_{0.8}\text{Fe}_{0.2}\text{O}_{3-\delta}$ synthesized by sol gel method using various chelating agents.

Table 3.20 Activation energy of $\text{Ba}_{0.5}\text{Sr}_{0.5}\text{Co}_{0.8}\text{Fe}_{0.2}\text{O}_{3-\delta}$ synthesized by sol gel method using various chelating agents

Sample	E_a (kJ/mol)
S-BSCF-MC	34.14
S-BSCF-G	34.46
S-BSCF-H ₅	35.36
S-BSCF-GC	34.84
S-BSCF-EC	34.92

3.2.3.2 Effect of chelating agents on the electrical conductivity of $\text{Ba}_{0.5}\text{Sr}_{0.5}\text{Co}_{0.8}\text{Fe}_{0.2}\text{O}_{3-\delta}$ synthesized by hydrothermal method

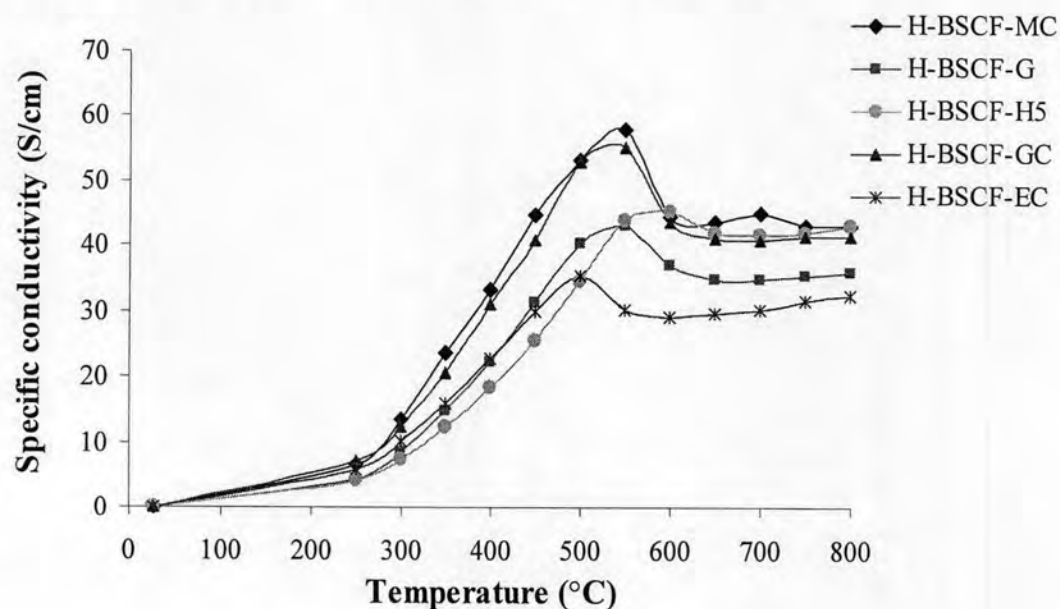


Figure 3.25 Variations of the electrical conductivity measured in air of $\text{Ba}_{0.5}\text{Sr}_{0.5}\text{Co}_{0.8}\text{Fe}_{0.2}\text{O}_{3-\delta}$ synthesized using various chelating agents with temperature.

The electrical conductivity of BSCF synthesized by hydrothermal method indicated a semi-conducting behavior of these materials at low temperature ($T \leq 550^\circ\text{C}$). Shown in Figure 3.25, the conductivity of H-BSCF specimen was lower than that of S-BSCF. The decrease in conductivity with decreasing grain sizes and the

density of H-BSCF (Table 3.11) was due to an increase in the concentration of the grain boundaries which had higher resistivity [36].

Shown in Table 3.21, the activation energy values of BSCF synthesized by hydrothermal method were calculated from the linear part of Figure 3.26. The activation energy of H-BSCF specimens was higher than that of S-BSCF.

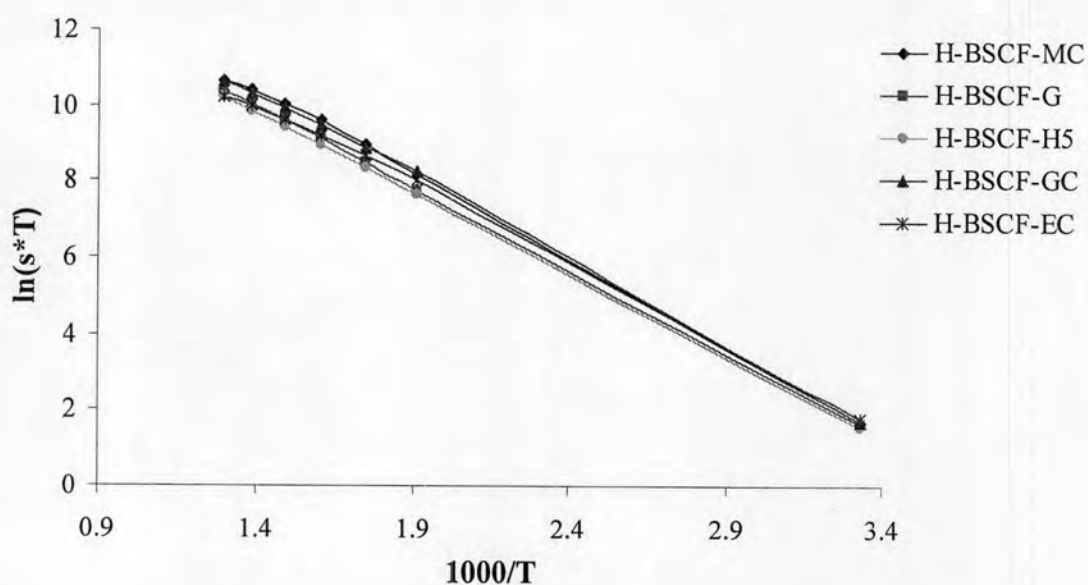


Figure 3.26 Arrhenius plot of $\text{Ba}_{0.5}\text{Sr}_{0.5}\text{Co}_{0.8}\text{Fe}_{0.2}\text{O}_{3-\delta}$ synthesized by hydrothermal method using various chelating agents.

Table 3.21 Activation energy of $\text{Ba}_{0.5}\text{Sr}_{0.5}\text{Co}_{0.8}\text{Fe}_{0.2}\text{O}_{3-\delta}$ synthesized by hydrothermal method using various chelating agents

Sample	E_a (kJ/mol)
H-BSCF-MC	36.47
H-BSCF-G	35.78
H-BSCF-H ₅	34.83
H-BSCF-GC	36.19
H-BSCF-EC	34.01

3.2.3.3 Effect of chelating agents on the electrical conductivity of PrSrCoO₄ synthesized by hydrothermal method

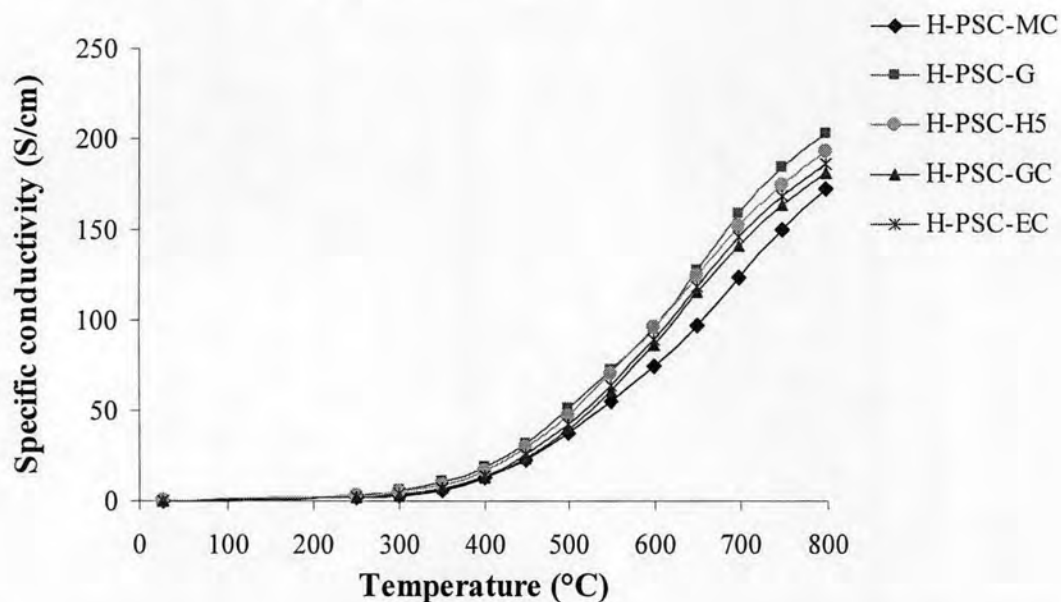


Figure 3.27 Variations of the electrical conductivity measured in air of PrSrCoO₄ synthesized using various chelating agents with temperature.

Figure 3.27 shows the electrical conductivity of PrSrCoO₄ synthesized by hydrothermal method using various chelating agents. The electrical conductivity of all compounds shows semi-conductor type in air in the temperature range from 25 to 800 °C. Chelating agents had slightly significant effect on the specific conductivity of PSC. However, H-PSC-G exhibited the highest conductivity (202.6 S/cm) at 800°C.

The logarithm of electrical conductivity versus reciprocal temperature in air is shown in Figure 3.28.

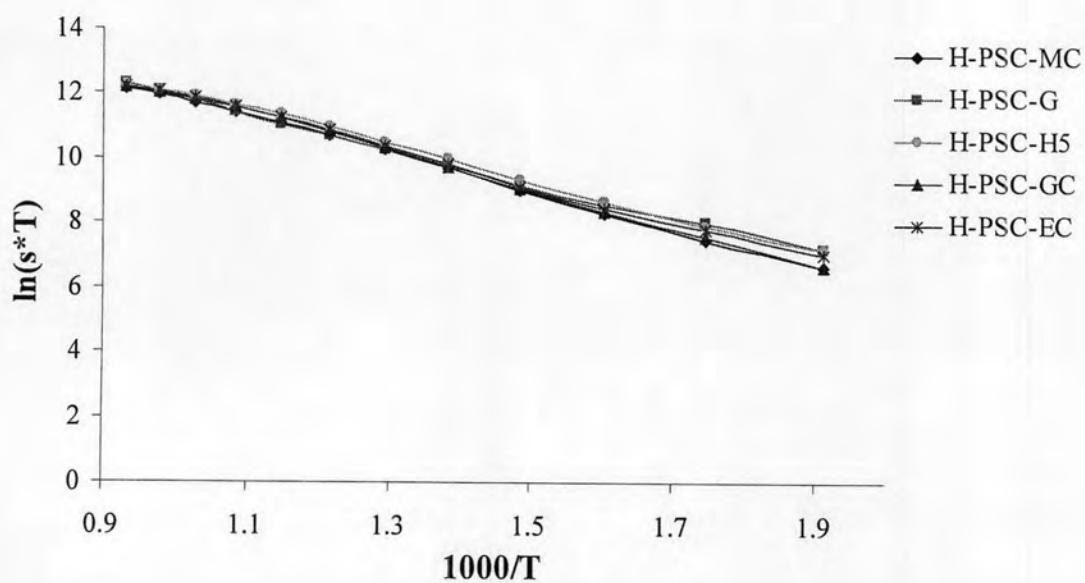


Figure 3.28 Arrhenius plot of PrSrCoO_4 synthesized by hydrothermal method using various chelating agents.

In Figure 3.28, the activation energy values of PrSrCoO_4 were calculated from the linear part of Arrhenius plots and the values are summarized in Table 3.22.

Table 3.22 Activation energy of PrSrCoO_4 synthesized by hydrothermal method using various chelating agents

Sample	E_a (kJ/mol)
H-PSC-MC	42.55
H-PSC-G	43.62
H-PSC-H ₅	44.84
H-PSC-GC	48.77
H-PSC-EC	42.27

3.2.3.4 Effect of chelating agents on the electrical conductivity of PrSrNiO₄ synthesized by hydrothermal method

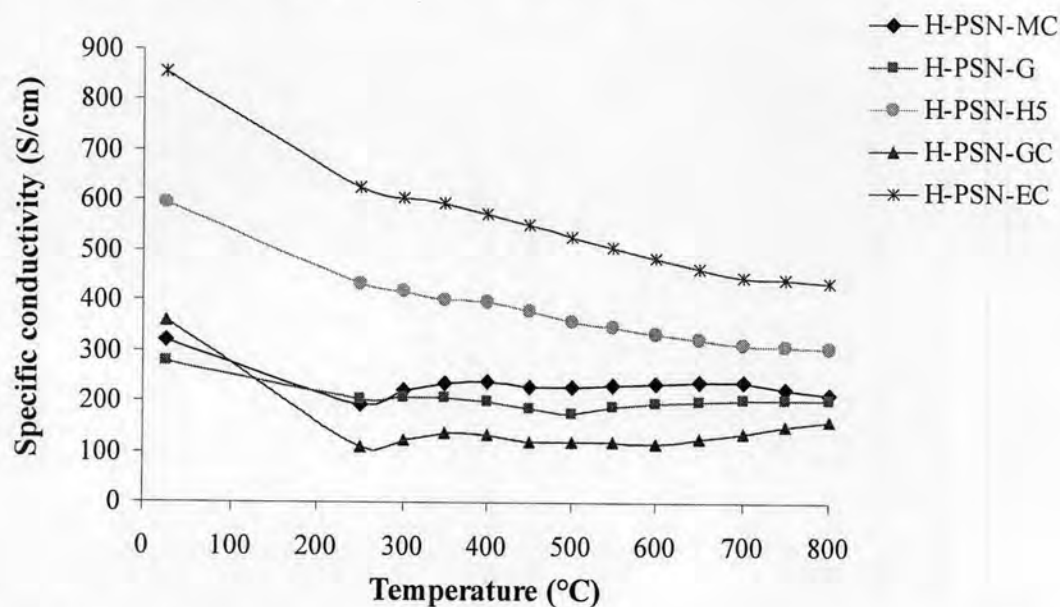


Figure 3.29 Variations of the electrical conductivity measured in air of PrSrNiO₄ synthesized using various chelating agents with temperature.

Figure 3.29 shows the electrical conductivity of the PrSrNiO₄ as a function of temperature. It is revealed that the conductivity of PSN decreased with temperature. These oxides behaved as a metallic material. Therefore, H-PSN-EC shows the maximum conductivity value (854.5 S/cm) at 27°C. Because of large grain size decreased concentration of grain boundaries. Although the number of grain boundaries per unit length decreased, the net effect on conductivity was higher than that for fine-grained microstructures. In case of H-PSN-MC, H-PSN-G and H-PSN-G, at temperature above 300°C, the conduction region was semiconductor-like.

Shown in Table 3.23, the activation energy of PrSrNiO₄ specimens was calculated from the linear part of Arrhenius plots (Figure 3.30). Activation energy of PrSrNiO₄ was significantly changed. However, H-PSN-H₅ displayed the lowest E_a due to the highest conductivity of its.

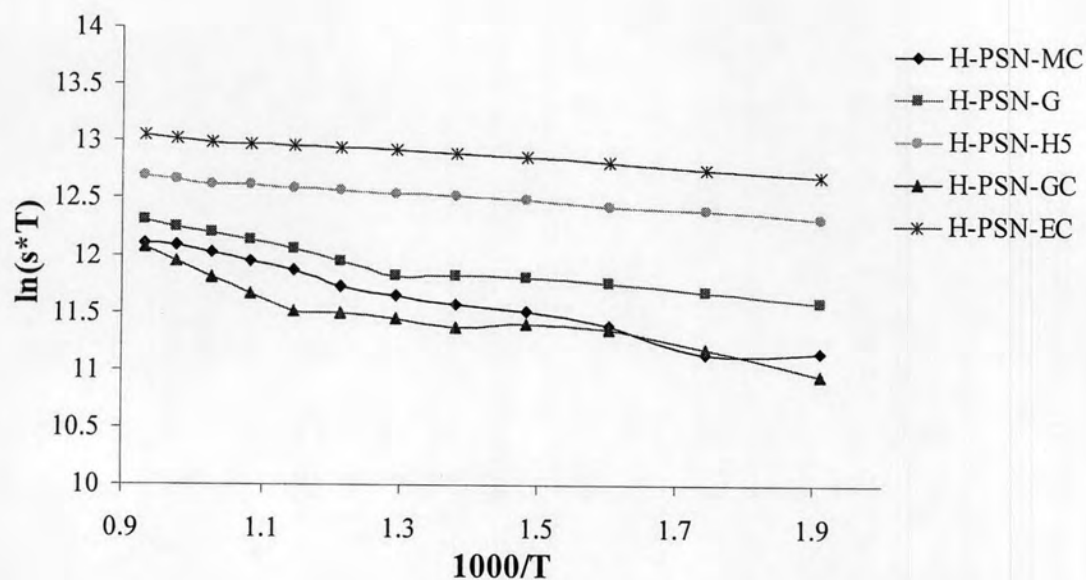


Figure 3.30 Arrhenius plot of PrSrNiO_4 synthesized by hydrothermal method using various chelating agents.

Table 3.23 Activation energy of PrSrNiO_4 synthesized by hydrothermal method using various chelating agents

Sample	E_a (kJ/mol)
H-PSN-MC	10.73
H-PSN-G	9.04
H-PSN-H ₅	2.74
H-PSN-GC	7.92
H-PSN-EC	2.80

3.2.3.5 Effect of chelating agents on the electrical conductivity of $\text{La}_{0.7}\text{Sr}_{0.3}\text{Ga}_{0.7}\text{Fe}_{0.2}\text{Mg}_{0.1}\text{O}_{3-\delta}$ synthesized by hydrothermal method

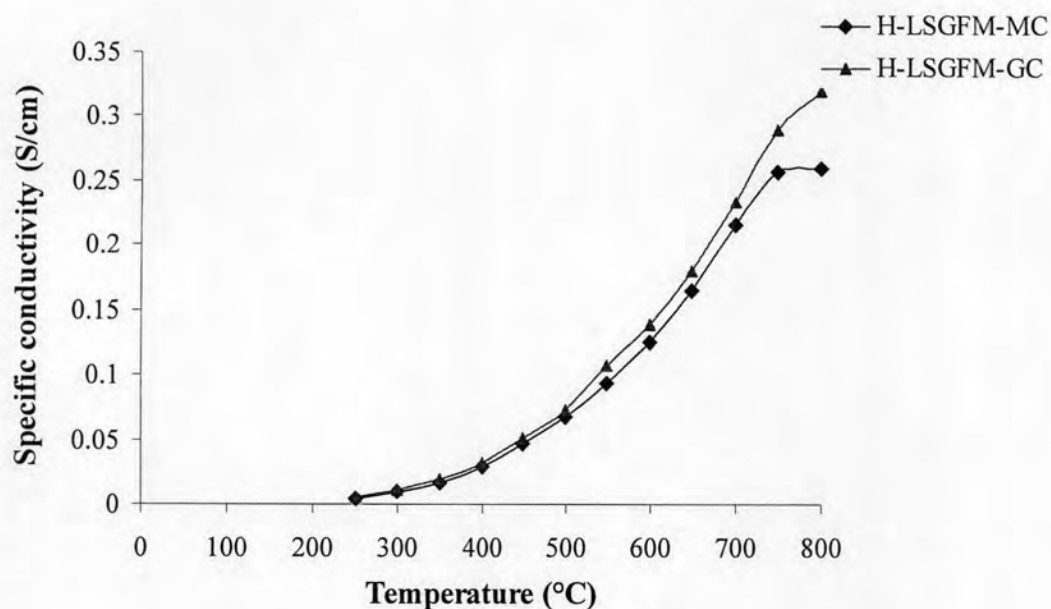


Figure 3.31 Variations of the electrical conductivity measured in air of $\text{La}_{0.7}\text{Sr}_{0.3}\text{Ga}_{0.7}\text{Fe}_{0.2}\text{Mg}_{0.1}\text{O}_{3-\delta}$ synthesized using various chelating agents with temperature.

As displayed in Figure 3.31, the maximum electrical conductivity of H-LSGFM-GC (0.32 S/cm at 800°C) was higher than that of H-LSGFM-MC (0.26 S/cm at 800°C). Similar to previous result, the higher grain size could cause the conductivity increasing.

Obtained from Figure 3.32, the activation energy of $\text{La}_{0.7}\text{Sr}_{0.3}\text{Ga}_{0.7}\text{Fe}_{0.2}\text{Mg}_{0.1}\text{O}_{3-\delta}$ is shown in Table 3.24, indicating that the activation energy of H-LSGFM-MC was lower than that of H-LSGFM-GC.

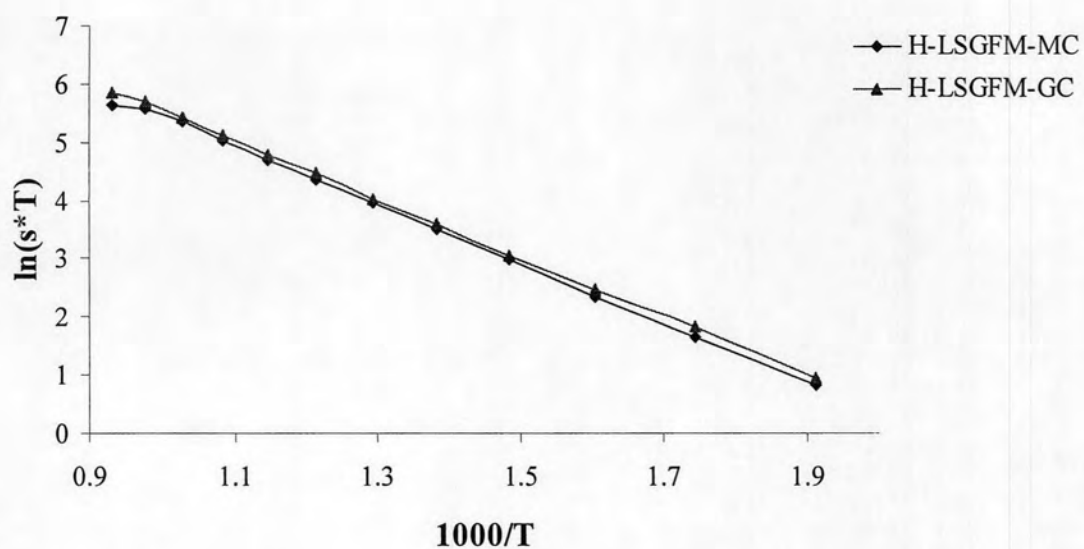


Figure 3.32 Arrhenius plot of $\text{La}_{0.7}\text{Sr}_{0.3}\text{Ga}_{0.7}\text{Fe}_{0.2}\text{Mg}_{0.1}\text{O}_{3-\delta}$ synthesized by hydrothermal method using various chelating agents.

Table 3.24 Activation energy of $\text{La}_{0.7}\text{Sr}_{0.3}\text{Ga}_{0.7}\text{Fe}_{0.2}\text{Mg}_{0.1}\text{O}_{3-\delta}$ synthesized by hydrothermal method using various chelating agents

Sample	E_a (kJ/mol)
H-LSGFM-MC	39.61
H-LSGFM-GC	39.00

3.2.3.6 Effect of chelating agents on the electrical conductivity of $\text{La}_{0.8}\text{Sr}_{0.2}\text{Ga}_{0.8}\text{Mg}_{0.15}\text{Co}_{0.05}\text{O}_{3-\delta}$ synthesized by hydrothermal method

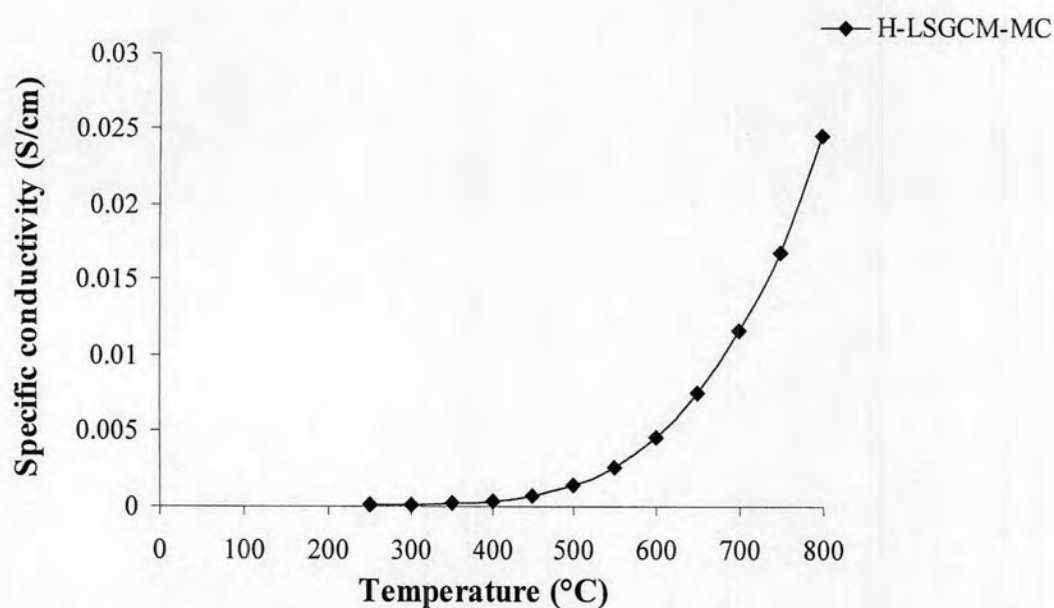


Figure 3.33 Variations of the electrical conductivity measured in air $\text{La}_{0.8}\text{Sr}_{0.2}\text{Ga}_{0.8}\text{Mg}_{0.15}\text{Co}_{0.05}\text{O}_{3-\delta}$ synthesized using various chelating agents with temperature.

Figure 3.33 show the electrical conductivity of $\text{La}_{0.8}\text{Sr}_{0.2}\text{Ga}_{0.8}\text{Mg}_{0.15}\text{Co}_{0.05}\text{O}_{3-\delta}$. In addition, Figure 3.34 and Table 3.25, the activation energy of $\text{La}_{0.8}\text{Sr}_{0.2}\text{Ga}_{0.8}\text{Mg}_{0.15}\text{Co}_{0.05}\text{O}_{3-\delta}$ was 66.58 kJ/mol.

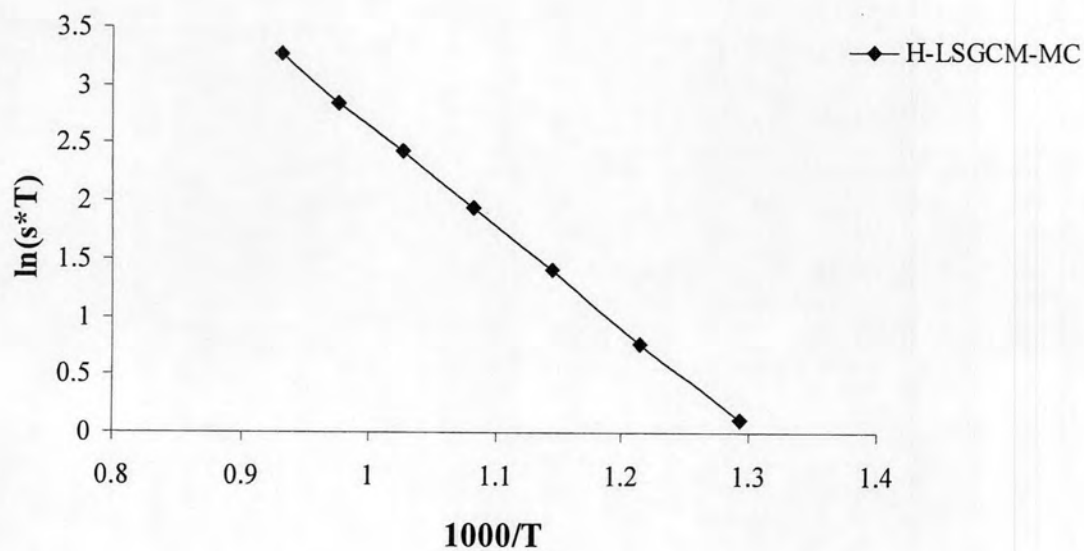


Figure 3.34 Arrhenius plot of $\text{La}_{0.8}\text{Sr}_{0.2}\text{Ga}_{0.8}\text{Mg}_{0.15}\text{Co}_{0.05}\text{O}_{3-\delta}$ synthesized by hydrothermal method using citric acid as a chelating agent.

Table 3.25 Activation energy of $\text{La}_{0.8}\text{Sr}_{0.2}\text{Ga}_{0.8}\text{Mg}_{0.15}\text{Co}_{0.05}\text{O}_{3-\delta}$ synthesized by hydrothermal method using citric acid as a chelating agent

Sample	E_a (kJ/mol)
H- LSGCM-MC	66.58

3.2.4 Thermal expansion coefficients

From the conductivity part, it is concluded that S-BSCF-EC, S-BSCF-EC, H-BSCF-MC, H-BSCF-GC, H-PSC-G, H-PSC-H₅, H-PSN-EC, H-PSN-H₅ exhibited the high conductivity. Thus, the other important properties of SOFC as TEC values were investigated. Thermal expansion coefficients were measured by NETZSCH DIL 402C dilatometer.

3.2.4.1 Effect of chelating agents on thermal expansion of Ba_{0.5}Sr_{0.5}



Figure 3.35 illustrates the thermal expansion of BSCF in air in the temperature range from room temperature to 800°C

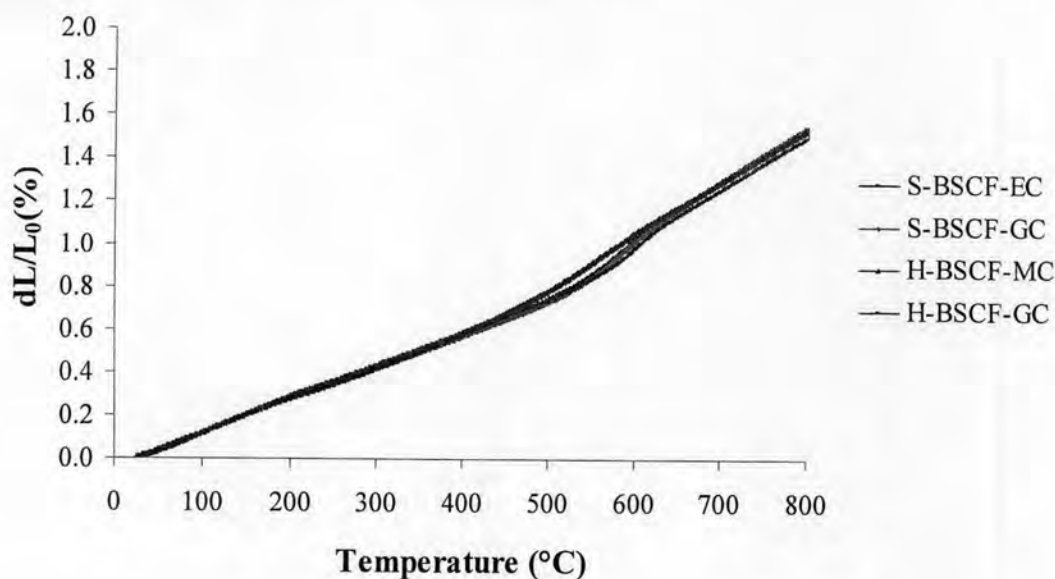
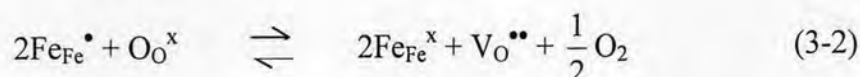
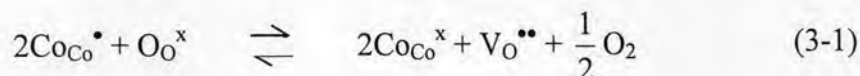


Figure 3.35 The thermal expansion curves for Ba_{0.5}Sr_{0.5}Co_{0.8}Fe_{0.2}O_{3-δ}.

The thermal expansion curves, shown in Figure 3.33 were linear, but they became steeper at elevated temperatures. The increase of the slope of the curves occurred about 490-570°C. This was caused by the loss of lattice oxygen and the formation of oxygen vacancies, a process which is enhanced as the repulsion force arising between those mutually exposed cations when oxygen ions are extracted from the lattice. Secondly, the increase in cation size due to the reduction of Co and Fe ions from higher (Co_{Co}[•] and Fe_{Fe}[•]) to lower valences (Co_{Co}^x and Fe_{Fe}^x), which must occur

concurrently with formation of oxygen vacancies ($V_{O}^{\bullet\bullet}$) in order to maintain electrical neutrality, described in equation (3-1) and (3-2) [37, 38, 39].



Thermal reduction of Co^{4+} , Fe^{4+} to Co^{3+} , Fe^{3+} was found to occur at about 490–570°C. The thermal expansion curves occurred turning around this temperature suggested the reduction of Co^{4+} and Fe^{4+} . Therefore, the formation of oxygen vacancies enhanced the thermal expansion coefficients. The thermal expansion coefficients of all samples are listed in Table 3.26

Table 3.26 The TEC values of $Ba_{0.5}Sr_{0.5}Co_{0.8}Fe_{0.2}O_{3-\delta}$

Sample	Temperature range	TEC $\times 10^{-6} (^{\circ}C^{-1})$	Source
BSCF	100-500	18.3415	Watcharin's thesis
	650-800	25.6417	
S-BSCF-EC	100-500	15.5519	This work
	700-800	25.3112	
S-BSCF-GC	100-500	15.2573	This work
	700-800	25.4621	
H-BSCF-GC	100-500	15.6436	This work
	700-800	24.4395	
H-BSCF-MC	100-500	16.4804	This work
	700-800	24.3653	

It is seen that the TEC values of both sol gel and hydrothermal method were reduced as compared with BSCF prepared by Watcharin's thesis [44]. Because of the particle size was decreased. In range of 700-800°C, the TEC values were slightly changed.

3.2.4.2 Effect of chelating agents on thermal expansion of PrSrCoO₄

The thermal expansion curves are shown in Figure 3.36 and TEC of the oxides are collected in Table 3.27. The thermal expansion coefficient of H-PSC-G and H-PSC-H₅ was lower than the TEC values that reported by Wang, Y. et al. [40].

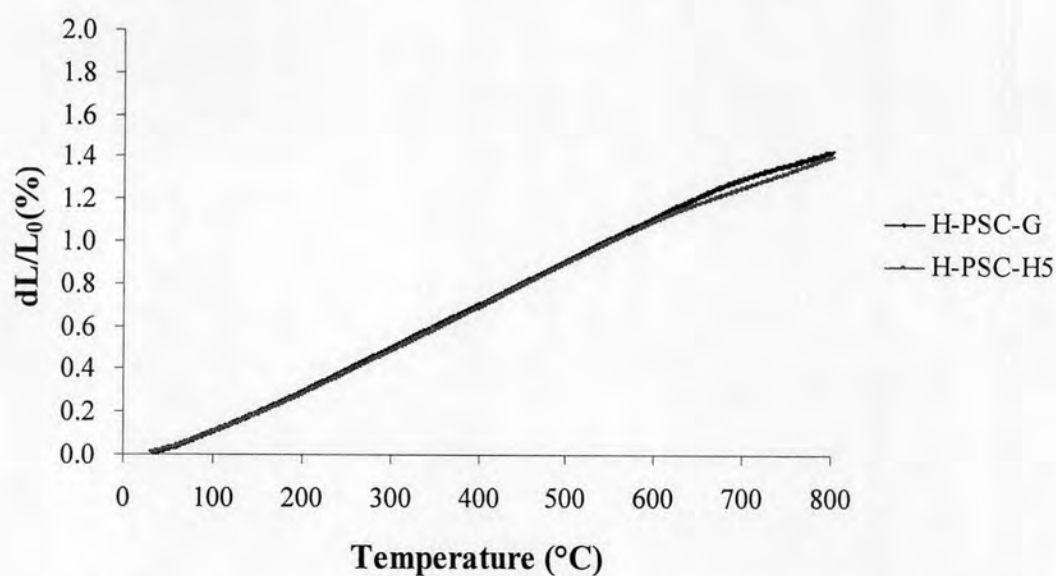


Figure 3.36 The thermal expansion curves for PrSrCoO₄ synthesized by hydrothermal method.

Table 3.27 The TEC values of PrSrCoO₄

Sample	Temperature range	TEC x10 ⁻⁶ (°C ⁻¹)	Source
PSC	30-1000	17.9	[40]
H-PSC-G	100-500	19.9749	This work
H-PSC-H ₅	100-500	19.7471	This work

3.2.4.3 Effect of chelating agents on thermal expansion of PrSrNiO₄

In Figure 3.37 and Table 3.28, It was found that both of PSN synthesized by hydrothermal method had the TEC values smaller than PSN that synthesized by Wen, T. et al. [41] affected by the reducing of the particle sizes.

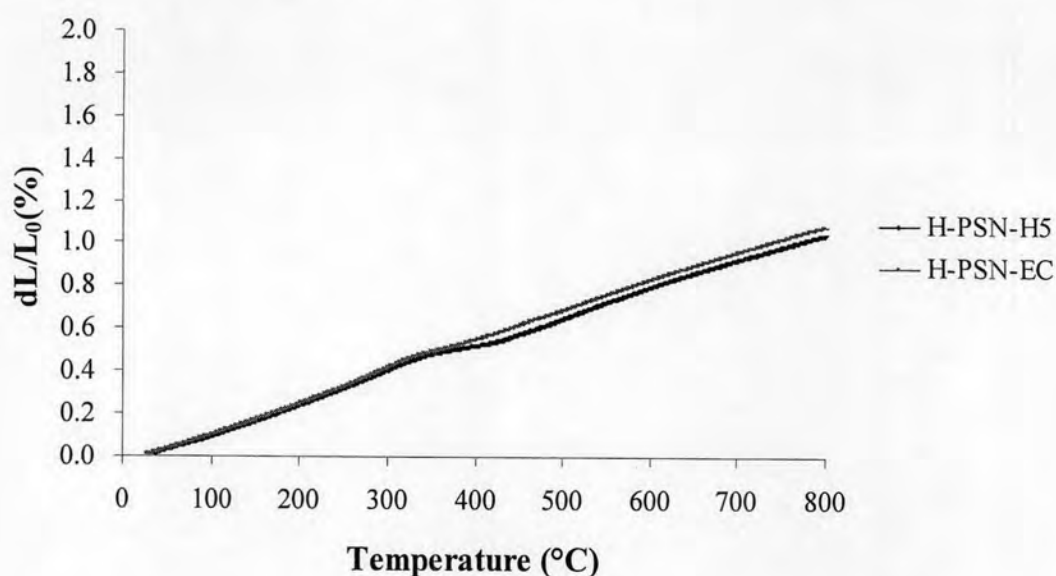


Figure 3.37 The thermal expansion curves for PrSrNiO₄ synthesized by hydrothermal method.

Table 3.28 The TEC values of PrSrNiO₄

Sample	Temperature range	TEC $\times 10^{-6} (^{\circ}\text{C}^{-1})$	Source
PrSr _{0.7} Ni _{0.3}	30-1000	15	[41]
PrSr _{0.4} Ni _{0.6}	30-1000	14.9	[41]
H-PSN-H ₅	100-500	13.8377	This work
	700-800	11.8786	
H-PSN-EC	100-500	14.6297	This work
	700-800	12.1900	

For LSGFM and LSGCM, the thermal expansion measurement was investigated on the sample that exhibited single phase structure.

3.2.4.4 Effect of chelating agents on thermal expansion of $\text{La}_{0.7}\text{Sr}_{0.3}$

$\text{Ga}_{0.7}\text{Fe}_{0.2}\text{Mg}_{0.1}\text{O}_{3.8}$

Figure 3.38 and Table 3.29 show the temperature dependence of the thermal expansion of $\text{La}_{0.7}\text{Sr}_{0.3}\text{Ga}_{0.7}\text{Fe}_{0.2}\text{Mg}_{0.1}\text{O}_{3.8}$. At lower temperature range (100-700°C), it was found that the TEC values of H-LSGFM-MC and H-LSGFM-GC were high as compared with [42].

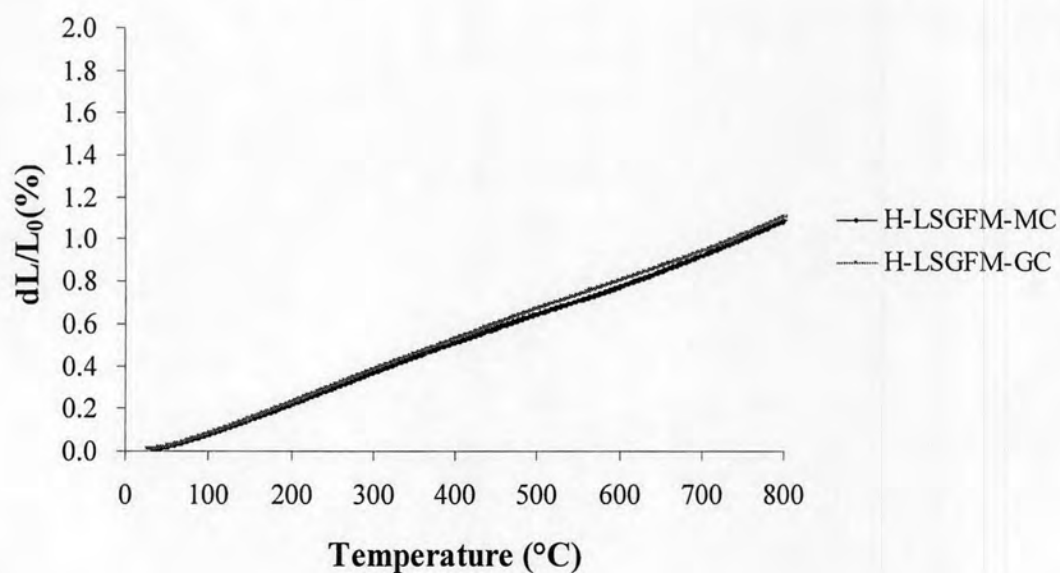


Figure 3.38 The thermal expansion curves for $\text{La}_{0.7}\text{Sr}_{0.3}\text{Ga}_{0.7}\text{Fe}_{0.2}\text{Mg}_{0.1}\text{O}_{3.8}$ synthesized by hydrothermal method.

Table 3.29 The TEC values of $\text{La}_{0.7}\text{Sr}_{0.3}\text{Ga}_{0.7}\text{Fe}_{0.2}\text{Mg}_{0.1}\text{O}_{3-\delta}$

Sample	Temperature range	TEC $\times 10^{-6} (\text{°C}^{-1})$	Source
$\text{La}_{0.8}\text{Sr}_{0.2}\text{Ga}_{0.6}\text{Mg}_{0.2}\text{Fe}_{0.2}\text{O}_{3-\delta}$	100-700	10.8	[42]
	700- 827	17.5	
H-LSGFM-MC	100-500	14.1057	This work
	700-800	16.6132	
H-LSGFM-GC	100-500	14.6827	This work
	700-800	16.2688	

3.2.4.5 Effect of chelating agents on thermal expansion of $\text{La}_{0.8}\text{Sr}_{0.2}$

$\text{Ga}_{0.8}\text{Mg}_{0.15}\text{Co}_{0.05}\text{O}_{3-\delta}$

The thermal expansion coefficient of H-LSGCM-MC was higher than the values from [42] due to the loss of lattice oxygen and the formation of oxygen vacancies.

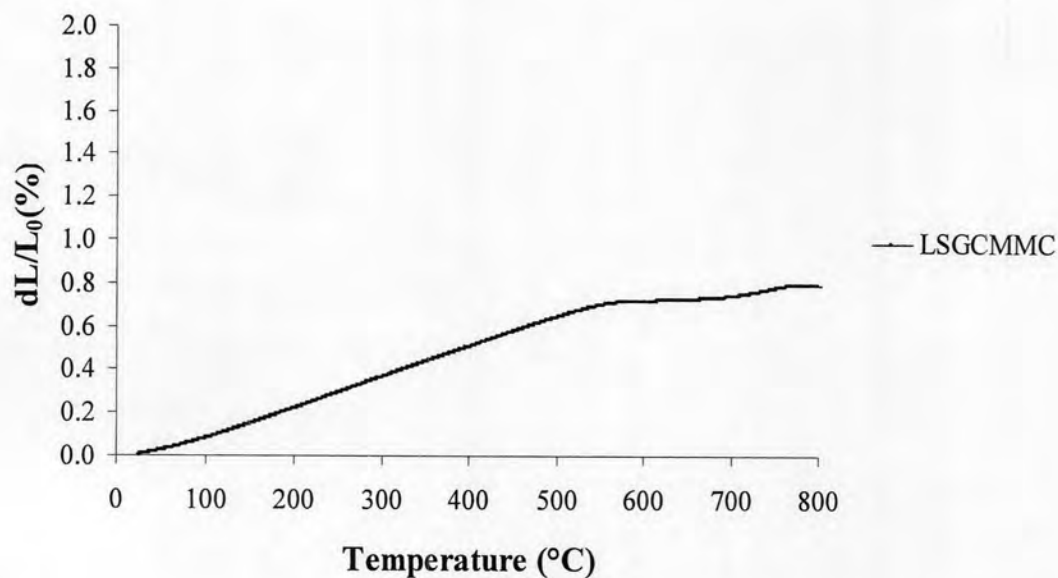


Figure 3.39 The thermal expansion curves for $\text{La}_{0.8}\text{Sr}_{0.2}\text{Ga}_{0.8}\text{Mg}_{0.15}\text{Co}_{0.05}\text{O}_{3-\delta}$ synthesized by hydrothermal method.

Table 3.30 The TEC values of $\text{La}_{0.8}\text{Sr}_{0.2}\text{Ga}_{0.8}\text{Mg}_{0.15}\text{Co}_{0.05}\text{O}_{3-\delta}$

Sample	Temperature range	TEC $\times 10^{-6} (\text{°C}^{-1})$	Source
$\text{La}_{0.8}\text{Sr}_{0.2}\text{Ga}_{0.6}\text{Mg}_{0.2}\text{Co}_{0.2}\text{O}_{3-\delta}$	100-687	13.4	[42]
	687-827	17.5	
H-LSGCM-MC	100-500	14.0485	This work
	700-800	5.4556	